Gradient-enhanced Coupled Plasticity-anisotropic Damage Model for Concrete Fracture: Computational Aspects and Applications

Rashid K. Abu Al-Rub*
Zachry Department of Civil Engineering, Texas A&M University College Station, TX 77843, USA

George Z. Voyiadjis
Department of Civil and Environmental Engineering, Louisiana State University, Baton Rouge, LA 70803, USA

ABSTRACT: It is widely studied that classical continuum damage theory for concrete fracture exhibits an extreme sensitivity to the spatial discretization in the finite element simulations. This sensitivity is caused by the fact that the mathematical description becomes ill-posed at a certain level of accumulated damage. A well-posed problem can be recovered by using a gradient-enhanced damage model in which a material length scale is introduced as a localization limiter. In this work, a nonlocal gradient-enhanced fully coupled plastic-damage constitutive model for plain concrete is developed. Anisotropic damage with a plasticity yield criterion and a damage criterion are introduced to be able to adequately describe the plastic and damage behavior of concrete. In order to account for different effects under tensile and compressive loadings, nonlocal damage variables that account for the progressive degradation of mechanical properties under stress states of prevailing tension and compression and two internal length scales, one for tension and the other for compression, are introduced as localization limiters. Therefore, two nonlocal damage criteria are used: one for compression and a second for tension such that the total stress is decomposed into tensile and compressive components. In order to solve the time step problem, a decoupled elastic predictor and plastic corrector steps are performed first in the effective configuration where damage is absent, and then a nonlocal damage corrector step is applied in order to update the final stress state. The algorithmic treatment of both tension and compression is presented in a unified way. A simple procedure to calculate the gradient of the tensile/compressive damage

*Author to whom correspondence should be addressed. E-mail: rabualrub@civil.tamu.edu
Figures 2–4, 7 and 11 appear in color online: http://ijd.sagepub.com

1056-7895/09/02 115–40 $10.00/0 DOI: 10.1177/1056789508097541

Los Angeles, London, New Delhi and Singapore

variables is described which can be used directly without the need of intensive numerical modifications of an existing finite element code. The effectiveness of the proposed local model has been demonstrated in both uniaxial and biaxial tension and compression problems and compared with experimental data. Numerical results obtained with the proposed nonlocal model are compared with experimental results concerning bending of three-point notched and four-point notched concrete beams. As the mesh is refined, convergence of numerical results is observed both in terms of damage patterns and of the global response.

KEY WORDS: nonlocal, damage mechanics, anisotropic damage, length scale, unilateral effect.

INTRODUCTION

Concrete is a widely used material in numerous engineering structures. The accurate modeling of its mechanical behavior under complex loading paths still represents a challenging task, especially when the prediction of failure is of interest. The distinct mechanical behavior of concrete in both tension and compression has increased the complexity of the constitutive modeling of its behavior. This distinct behavior is attributed to the different microdamage mechanisms during tensile and compressive loading conditions. The degradation in the concrete mechanical properties (i.e., damage) can be effectively modeled using the framework of continuum damage mechanics: isotropic (scalar) damage models with one or two (one for tension and one for compression) damage variables (e.g., Krajcinovic, 1983, 1985; Mazars and Pijaudier-Cabot, 1989; Lubliner et al., 1989; Lubarda et al., 1994; Faria et al., 1998; Lee and Fenves, 1998; Peerlings et al., 1998; Comi, 2001; Jason et al., 2004, 2006; Wu et al., 2006), anisotropic (tensor) damage models (e.g., Dragon and Mroz, 1979; Sidoroff, 1981; Krajcinovic and Fonseka, 1981; Ortiz, 1985; Simo and Ju, 1987a, b; Ju, 1989, 1990; Valanis, 1991; Ramtani et al., 1992; Lubarda and Krajcinovic, 1993; Voyiadjis and Abu-Lebdeh, 1994; Yazdani and Schreyer, 1994; Govindjee et al., 1995; Halm and Dragon, 1996; Fichant et al., 1999; Carol et al., 2001; Hansen et al., 2001; Gatuingt and Pijaudier-Cabot; 2002; Cicekli et al., 2007).

However, it is widely studied when using the local damage models that as soon as material failure dominates a deformation process, the material increasingly displays strain softening (localization) and the finite element computations are considerably affected by the mesh size and alignment and gives nonphysical descriptions of the damaged regions and failure of structures such that the size of the fracture process zone is controlled by the size of one element in a finite element context. In other words, the boundary

value problem in the presence of damage-induced softening may become ill-posed. For quasi-static loading conditions, well-posed solutions can be obtained by enhancing the local damage models by nonlocal measure(s). This can be achieved either by using the nonlocal integral approach (e.g., Pijaudier-Cabot and Bazant, 1987; Bazant and Pijaudier-Cabot, 1988; Comi, 2001; Ferrara and di Prisco, 2001) or the gradient-enhanced approach (see e.g., Aifantis, 1984; Lasry and Belytschko, 1988; Zbib and Aifantis, 1992; de Borst and Mühlhaus, 1992; Peerlings et al., 1996, 1998; de Borst et al., 1993, 1999; de Borst and Pamin, 1996; Comi and Perego, 1996; Svedberg and Runesson, 2000; Askes et al., 2000; Kuhl et al., 2000; Geers et al., 2000; Nedjar, 2001; Chen and Yuan, 2002; Liebe et al., 2003; Voyiadjis et al., 2001, 2003, 2004; Abu Al-Rub and Voyiadjis, 2006; and the references quoted therein). In this article the later approach is used within a continuum damage mechanics framework. In the nonlocal models the explicit incorporation of a material length scale fixes the width of the damaged zone, thus preventing strain localization into a line with consequent zero energy dissipation (Abu Al-Rub, 2004).

The nonlinear material behavior of concrete can be attributed to two distinct material mechanical processes: damage and plasticity. These two degradation phenomena may be described best by the theories of continuum damage mechanics and plasticity. One type of combination relies on stress-based plasticity formulated in the effective (undamaged) space (e.g., Simo and Ju, 1987a, b; Ju, 1989, 1990; Yazdani and Schreyer, 1990; Lee and Fenves, 1998; Gatuingt and Pijaudier-Cobot, 2002; Jason et al., 2004; Wu et al., 2006; Cicekli et al., 2007), where the effective stress is defined as the average microscale stress acting on the undamaged material between microdefects. Another type is based on stress-based plasticity in the nominal (damaged) stress space (e.g., Bazant and Kim, 1979; Ortiz, 1985; Lubliner et al., 1989; Imran and Pantazopoulu, 2001; Ananiev and Ozbolt, 2004; Kratzig and Polling, 2004), where the nominal stress is defined as the macroscale stress acting on both damaged and undamaged material. However, it is shown by Abu Al-Rub and Voyiadjis (2004) that coupled plastic-damage models formulated in the effective space are numerically more stable and attractive. On the other hand, for better characterization of the concrete damage behavior, anisotropic damage effects, i.e., different microcracking in different directions, should be characterized (Ju, 1990). However, anisotropic damage in concrete is complex and the coupling with plasticity and the application to structural analysis is not straightforward (e.g., Ju, 1989, 1990; Yazdani and Schreyer, 1990; Voyiadjis and Abu-Lebdeh, 1994; Meschke et al., 1998; Voyiadjis and Kattan, 1999; Carol et al., 2001; Hansen et al., 2001; Cicekli et al., 2007), and therefore, it has been avoided by many authors.

The coupled anisotropic damage and plasticity constitutive model of Cicekli et al. (2007) is successfully used to predict the concrete distinct behavior in tension and compression and is formulated within the basic principles of thermodynamics. In this article, this model is adapted and enhanced with nonlocal gradient-dependent damage variables. The nonlocality is enhanced by adding to the local tensile/compressive damage variables an additional term that involves a material length scale and the Laplacian (i.e., second-order gradient) of the local tensile/compressive damage variables. Since the damage mechanism in tension is very different than in compression, two distinct material length scales are incorporated, one for tension and one for compression, which are related to the width of the localized band for stress states of prevailing tension or compression. Pertinent computational aspects concerning the algorithmic aspects and numerical implementation of the proposed nonlocal constitutive model in the well-known finite element code ABAQUS (2003) are presented. The algorithmic treatment of both tension and compression is presented in a unified way. In order to solve the time step problem, a decoupled elastic predictor and plastic corrector steps are performed first in the effective configuration where damage is absent, and then a nonlocal damage corrector step is applied in order to update the final stress state. A simple procedure to calculate the Laplacians of the tensile/compressive damage variables is described which can be used directly without the need of intensive numerical modifications of an existing finite element code. The computation of the Laplacian is based on a least-square polynomial approximation of the damage consistency multiplier around each integration point. This nonlocal return mapping algorithm allows satisfying exactly the plasticity and damage consistency conditions in a point-wise fashion at each iteration of a load step. Numerical results obtained with the proposed nonlocal model are compared with experimental results concerning bending of three-point notched and four-point notched concrete beams.

LOCAL ANISOTROPIC PLASTIC-DAMAGE MODEL

In this section, the local coupled plasticity-damage model that has been recently formulated by Cicekli et al. (2007) for plain concrete based on the laws of thermodynamics is presented. This model includes the Lubliner plasticity yield criterion (Lubliner et al., 1989; Lee and Fenves, 1998) expressed in the effective (undamaged) space; nonassociative plasticity flow rule based on the Drucker-Prager potential; and two damage evolution surfaces, one for tensile damage and the other for compressive damage. Damage anisotropy is different in tension and in compression. Thus, this

model characterizes the damage anisotropy by two damage second-order tensors, φ_{ij}^{+} and φ_{ij}^{-}, that measure damage under stress states of prevailing tension and of prevailing compression, respectively. This model will be enhanced in 'Enhancement of Nonlocal Damage Anisotropy in Concrete' section by nonlocal gradient-dependent damage variables.

In formulating this model, the effective (undamaged) configuration concept (Kachonov, 1958) is used such that the damaged material is modeled using the constitutive laws of the effective undamaged material in which the Cauchy stress tensor, σ_{ij}, is replaced by the effective stress tensor, $\bar{\sigma}_{ij}$ (e.g., Cordebois and Sidoroff, 1979; Murakami and Ohno, 1981; Simo and Ju, 1987a; Voyiadjis and Kattan, 1999):

$$\bar{\sigma}_{ij} = M_{ijkl}\sigma_{kl} \tag{1}$$

with M_{ijkl} being the fourth-order damage-effect tensor and is related to the second-order tensor φ_{ij} through the following expression outlined in Abu Al-Rub and Voyiadjis (2003):

$$M_{ijkl} = 2\left[(\delta_{ij} - \varphi_{ij})\delta_{kl} + \delta_{ij}(\delta_{kl} - \varphi_{kl})\right]^{-1} \tag{2}$$

It will be shown in the subsequent development that M_{ijkl} can be expressed in terms of both φ_{ij}^{+} and φ_{ij}^{-}. In the subsequence of this article, the superimposed dash designates a variable in the effective (undamaged) configuration and + to designate tension and – to designate compression.

The transformation from the effective configuration to the damaged one can be done by utilizing either the strain equivalence or strain energy equivalence hypotheses (Lemaitre, 1992). However, in this work the strain equivalence hypothesis is adopted for simplicity, which basically states that the strains in the damaged configuration and the strains in the undamaged configuration are equal (Lemaitre, 1992). This assumption introduces a great simplicity in the computational implementation as will be shown in 'Numerical Integration of the Constitutive Model' section. Therefore, the total strain tensor ε_{ij} is set equal to the corresponding effective tensor $\bar{\varepsilon}_{ij}$ (i.e. $\varepsilon_{ij} = \bar{\varepsilon}_{ij}$), which can be decomposed into an elastic strain $\varepsilon_{ij}^{\mathrm{e}}$ (or $\bar{\varepsilon}_{ij}^{\mathrm{e}}$) and a plastic strain $\varepsilon_{ij}^{\mathrm{p}}$ (or $\bar{\varepsilon}_{ij}^{\mathrm{p}}$) such that:

$$\varepsilon_{ij} = \varepsilon_{ij}^{\mathrm{e}} + \varepsilon_{ij}^{\mathrm{p}} = \bar{\varepsilon}_{ij}^{\mathrm{e}} + \bar{\varepsilon}_{ij}^{\mathrm{p}} = \bar{\varepsilon}_{ij} \tag{3}$$

Using the generalized Hooke's law, the effective stress is given as follows:

$$\bar{\sigma}_{ij} = \bar{E}_{ijkl}\left(\varepsilon_{kl} - \varepsilon_{kl}^{\mathrm{p}}\right) \tag{4}$$

where $\bar{E}_{ijkl}$ is the fourth-order undamaged elastic stiffness tensor. For isotropic linear-elastic materials, $\bar{E}_{ijkl}$ is given by:

$$\bar{E}_{ijkl} = 2\bar{G}I^{\mathrm{d}}_{ijkl} + \bar{K}I_{ijkl} \tag{5}$$

where $I^{\mathrm{d}}_{ijkl} = I_{ijkl} - (1/3)\delta_{ij}\delta_{kl}$ is the deviatoric part of the fourth-order identity tensor $I_{ijkl} = (1/2)(\delta_{ik}\delta_{jl} + \delta_{il}\delta_{jk})$, and $\bar{G} = \bar{E}/2(1+\nu)$ and $\bar{K} = \bar{E}/3(1-2\nu)$ are the effective shear and bulk moduli, respectively, with $\bar{E}$ being the Young's modulus and ν the Poisson's ratio that are obtained from the stress–strain diagram in the effective configuration.

Similarly, in the damaged (nominal) configuration the stress–strain relationship in Equation (4) can be expressed by:

$$\sigma_{ij} = E_{ijkl}\left(\varepsilon_{kl} - \varepsilon^{\mathrm{p}}_{kl}\right) \tag{6}$$

By comparing Equations (4) and (6) and making use of Equations (1) and (3), one can express the damaged elasticity tensor E_{ijkl} in terms of the corresponding undamaged elasticity tensor $\bar{E}_{ijkl}$ by the following relation:

$$E_{ijkl} = M^{-1}_{ijmn}\bar{E}_{mnkl} \tag{7}$$

Plasticity Yield Criterion

The Lubliner plasticity yield criterion (Lubliner et al., 1989; Lee and Fenves, 1998), which accounts for both tension and compression plasticity, can be expressed in the effective (undamaged) configuration as follows:

$$f = \sqrt{3\bar{J}_2} + \alpha\bar{I}_1 + \beta(\kappa^-,\kappa^+)H(\hat{\bar{\sigma}}_{\max})\hat{\bar{\sigma}}_{\max} - (1-\alpha)c^-(\kappa^-) \le 0 \tag{8}$$

where $\bar{J}_2 = \bar{s}_{ij}\bar{s}_{ij}/2$ is the second invariant of the effective deviatoric stress $\bar{s}_{ij} = \bar{\sigma}_{ij} - \bar{\sigma}_{kk}\delta_{ij}/3$, $\bar{I}_1 = \bar{\sigma}_{kk}$ is the first invariant of the effective Cauchy stress tensor $\bar{\sigma}_{ij}$.

In Equation (8), $\hat{\bar{\sigma}}_{\max}$ is the maximum principal effective stress, $H(\hat{\bar{\sigma}}_{\max})$ is the Heaviside step function ($H=1$ for $\hat{\bar{\sigma}}_{\max} > 0$ and $H=0$ for $\hat{\bar{\sigma}}_{\max} < 0$), and the parameters α and β are dimensionless constants which are defined as follows:

$$\alpha = \frac{(f_{b0}/f_0^-) - 1}{2(f_{b0}/f_0^-) - 1}, \quad \beta = (1-\alpha)\frac{c^-(\kappa^-)}{c^+(\kappa^+)} - (1+\alpha) \tag{9}$$

with f_{b0} and f_0^- being the initial equibiaxial and uniaxial compressive yield stresses, respectively. Experimental values for f_{b0}/f_0^- lie between 1.10 and 1.16; yielding α between 0.08 and 0.12. The variables $\kappa^+ = \int_0^t \dot{\kappa}^+ \mathrm{d}t$ and $\kappa^- = \int_0^t \dot{\kappa}^- \mathrm{d}t$ are the equivalent plastic strains in tension and compression, respectively, and their rates are defined as follows:

$$\dot{\kappa}^+ = r(\hat{\bar{\sigma}}_{ij})\hat{\dot{\varepsilon}}^{\mathrm{p}}_{\max}, \quad \dot{\kappa}^- = -(1 - r(\hat{\bar{\sigma}}_{ij}))\hat{\dot{\varepsilon}}^{\mathrm{p}}_{\min} \tag{10}$$

where $\hat{\dot{\varepsilon}}^{\mathrm{p}}_{\max}$ and $\hat{\dot{\varepsilon}}^{\mathrm{p}}_{\min}$ are the maximum and minimum principal values of the plastic strain rate $\dot{\varepsilon}^{\mathrm{p}}_{ij}$ such that $\hat{\dot{\varepsilon}}^{\mathrm{p}}_1 > \hat{\dot{\varepsilon}}^{\mathrm{p}}_2 > \hat{\dot{\varepsilon}}^{\mathrm{p}}_3$ with $\hat{\dot{\varepsilon}}^{\mathrm{p}}_{\max} = \hat{\dot{\varepsilon}}^{\mathrm{p}}_1$ and $\hat{\dot{\varepsilon}}^{\mathrm{p}}_{\min} = \hat{\dot{\varepsilon}}^{\mathrm{p}}_3$. Note that the superscript $+$ or $-$ designates a tensile or compressive quantity, and $(\hat{\bullet})$ designates the principle value of $(\bullet)$. The dimensionless parameter $r(\hat{\bar{\sigma}}_{ij})$ is a weight factor depending on principal stresses and is defined as follows:

$$r(\hat{\bar{\sigma}}_{ij}) = \frac{\sum_{k=1}^{3} \langle \hat{\bar{\sigma}}_k \rangle}{\sum_{k=1}^{3} \left| \hat{\bar{\sigma}}_k \right|} \tag{11}$$

where $\langle\ \rangle$ is the Macauley bracket presented as $\langle x \rangle = 1/2(|x| + x)$. Note that $r(\hat{\bar{\sigma}}_{ij}) = r(\hat{\sigma}_{ij})$. Moreover, depending on the value of $r(\hat{\bar{\sigma}}_{ij})$: (a) in case of uniaxial tension $\hat{\bar{\sigma}}_k \geq 0$ and $r(\hat{\bar{\sigma}}_{ij}) = 1$, and (2) in case of uniaxial compression $\hat{\bar{\sigma}}_k \leq 0$ and $r(\hat{\bar{\sigma}}_{ij}) = 0$.

In the last term of Equation (8), the function c^- represents the material cohesion in uniaxial compression. Since the concrete behavior in compression is more of a ductile behavior as compared to its corresponding brittle behavior in tension, the evolution of the compressive and tensile isotropic hardening functions c^- and c^+ are defined by the following exponential and linear hardening laws, respectively:

$$c^- = f_0^- + Q[1 - \exp(-b\kappa^-)], \quad c^+ = f_0^+ + h\kappa^+ \tag{12}$$

where f_0^- and f_0^+ are the initial yield stresses in compression and tension (i.e., when nonlinear behavior starts), respectively. The parameters Q, b, and h are material constants, which are obtained in the effective configuration of the uniaxial stress–strain diagram.

For realistic modeling of the volumetric expansion under compression for concrete, a non-associative plasticity flow rule should be used. This can be done by writing the evolution of the plastic strain tensor, $\dot{\varepsilon}^{\mathrm{p}}_{ij}$, in terms of a plastic potential F^{p} that is not equal to the plastic yield function f such that:

$$\dot{\varepsilon}^{\mathrm{p}}_{ij} = \dot{\lambda}^{\mathrm{p}} \frac{\partial F^{\mathrm{p}}}{\partial \bar{\sigma}_{ij}} \tag{13}$$

where $\dot{\lambda}^{\mathrm{p}}$ is the plastic multiplier, which can be obtained using the plasticity consistency condition, $\dot{f} = 0$, such that:

$$f \leq 0, \quad \dot{\lambda}^{\mathrm{p}} \geq 0, \quad \dot{\lambda}^{\mathrm{p}} f = 0, \quad \dot{\lambda}^{\mathrm{p}} \dot{f} = 0 \tag{14}$$

The plastic potential F^{p} can be expressed in terms of the Drucker-Prager function as:

$$F^{\mathrm{p}} = \sqrt{3\bar{J}_2} + \alpha^{\mathrm{p}} \bar{I}_1 \tag{15}$$

where α^{p} is the dilation material constant.

Tensile and Compressive Damage Surfaces

The anisotropic damage growth function proposed by Chow and Wang (1987) and used my many others (see e.g., Abu Al-Rub and Voyiadjis, 2003, 2006; Voyiadjis et al., 2003, 2004, 2006, and the references quoted therein) is adopted in this study. However, this function is generalized in Cicekli et al. (2007) in order to incorporate both tensile and compressive damage separately, such that:

$$g^{\pm} = \sqrt{\frac{1}{2} Y^{\pm}_{ij} L^{\pm}_{ijkl} Y^{\pm}_{ij}} - K^{\pm}(\omega^{\pm}) \leq 0 \tag{16}$$

where the superscript $\pm$ designates tension, $+$, or compression, $-$, $K^{\pm}$ is the tensile or compressive damage isotropic hardening function, $K^{\pm} = K^{\pm}_0$ when there is no damage, where $K^{\pm}_0 = f^{\pm 2}_0 / 2\bar{E}$ is the tensile or compressive initial damage parameter (i.e., damage threshold), L_{ijkl} is a fourth-order symmetric tensor, and Y_{ij} is the damage driving force that characterizes damage evolution and is interpreted as the energy release rate. In order to simplify the anisotropic damage formulation, L_{ijkl} is taken in this work as the fourth-order identity tensor I_{ijkl}.

The rate of the equivalent damage $\dot{\omega}^{\pm}$ (i.e., rate of damage accumulation) is defined as:

$$\dot{\omega}^{\pm} = \sqrt{\dot{\varphi}^{\pm}_{ij} \dot{\varphi}^{\pm}_{ij}} \quad \text{with} \quad \omega^{\pm} = \int_0^t \dot{\omega}^{\pm} \, \mathrm{d}t \tag{17}$$

The evolution equation for $\dot{\varphi}^{\pm}_{ij}$ is defined by:

$$\dot{\varphi}^{\pm}_{ij} = \dot{\lambda}^{\pm}_{\mathrm{d}} \frac{\partial g^{\pm}}{\partial Y^{\pm}_{ij}} \tag{18}$$

where $\dot{\lambda}^{\pm}_{\mathrm{d}}$ is the damage multiplier such that one can easily show from Equations (16)–(18) that $\dot{\lambda}^{\pm}_{\mathrm{d}} = \dot{\omega}^{\pm}$. This multiplier can be obtained from the

damage consistency condition:

$$g^{\pm} \leq 0,\ \dot{\lambda}_{\mathrm{d}}^{\pm} g^{\pm} = 0, \quad \text{and} \quad \dot{g}^{\pm} \begin{cases} < 0 \Rightarrow \dot{\lambda}_{\mathrm{d}}^{\pm} = 0 \\ = 0 \Rightarrow \dot{\lambda}_{\mathrm{d}}^{\pm} \geq 0 \end{cases}$$
$$\Leftrightarrow \begin{cases} \text{effective (undamaged state)} \\ \text{damage initiation/growth} \end{cases} \tag{19}$$

The evolution of the tensile and compressive damage isotropic hardening functions, $\dot{K}^{+}$ and $\dot{K}^{-}$, are defined as follows:

$$\dot{K}^{+} = \frac{K^{+}}{B^{+} + (K_0^{+}/K^{+})} \exp\left[-B^{+}\left(1 - \frac{K^{+}}{K_0^{+}}\right)\right]\dot{\omega}^{+},$$
$$\dot{K}^{-} = \frac{K_0^{-}}{B^{-}} \exp\left[-B^{-}\left(1 - \frac{K^{-}}{K_0^{-}}\right)\right]\dot{\omega}^{-} \tag{20}$$

where $B^{\pm}$ is a material constant, which is related to the tensile and compressive fracture energies, and therefore can be calibrated from the uniaxial tensile and compressive stress–strain diagrams.

The damage driving force $Y_{ij}^{\pm}$ can be expressed as follows:

$$Y_{ij}^{\pm} = -\frac{1}{2} \bar{E}_{rsab}^{-1} \bar{\sigma}_{ab}^{\pm} \frac{\partial (M_{rspq}^{\pm})^{-1}}{\partial \varphi_{ij}^{\pm}} \bar{\sigma}_{pq}^{\pm} \tag{21}$$

where the spectral decomposition of the effective stress into tensile and compressive parts, $\bar{\sigma}_{ij}^{+}$ and $\bar{\sigma}_{ij}^{-}$, will be shown in the next section.

It is noteworthy that for tensile loading, damage and plasticity are initiated when the equivalent applied stress reaches the ultimate tensile strength f_{u}^{+} whereas under compressive loading, damage is initiated earlier than plasticity. Once the equivalent applied stress reaches f_0^{-} (i.e., when nonlinear behavior starts) damage is initiated, whereas plasticity occurs once the ultimate compressive strength, f_{u}^{-}, is reached. Therefore, generally $f_0^{+} = f_{\mathrm{u}}^{+}$ for tensile loading, but this is not true for compressive loading (i.e., $f_0^{-} \neq f_{\mathrm{u}}^{-}$). However, one may obtain $f_0^{-} \approx f_{\mathrm{u}}^{-}$ in case of ultra-high strength concrete.

ENHANCEMENT OF NONLOCAL DAMAGE ANISOTROPY IN CONCRETE

The proposed enhanced version of the above model is based on the concept of nonlocal damage. Generally, as stated in the introduction section,

there are two approaches to enhance nonlocality: (a) either by using the nonlocal integral weighted average, (b) or by using the gradient-dependent form. The gradient-dependent approach is here exploited in view of a simple and attractive numerical treatment.

Proposed Damage Nonlocality

It can be noted that the Kachonov's mathematical definition of the effective stress in Equation (1) may be interpreted as the average stress acting on an effective area of the material. In order to give it a general physical meaning, it is necessary to use the corresponding damage-free material (i.e., virgin material) in the mesoscale to represent the 'effective' concept of Equation (1) for a macroscopically damaged material. Thus, a proper correlating hypothesis between the two material scale levels, the meso- and macroscales, can be obtained by enhancing nonlocality through using a nonlocal measure for both the tensile and compressive damage variables, $\widehat{\varphi}_{ij}^{+}$ and $\widehat{\varphi}_{ij}^{-}$, where the superimposed hat indicates a nonlocal quantity. It is then important to emphasize that Kachonov's definition given by Equation (1) can be generalized to a nonlocal one, for the case of anisotropic damage and under a general state of stress, as follows:

$$\bar{\sigma}_{ij} = \widehat{M}_{ijkl}\sigma_{kl} \tag{22}$$

where $\widehat{M}_{ijkl}$ is the nonlocal damage-effect tensor, which is a function of the nonlocal damage variable $\widehat{\varphi}_{ij}^{\pm}$. This functionality is described in the subsequent developments.

Furthermore, since the strain-softening behavior in concrete, whether in tension or compression, is driven by damage evolution processes, characterizing damage in terms of a nonlocal variable is more suitable for eliminating the mesh-dependency in the computer simulations of localized damage. In this article, $\widehat{\varphi}_{ij}^{\pm}$ characterizes the notion of nonuniform distribution and interaction of microdamages (microcracks and microvoids) over multiple length scales at which first and second nearest neighbor effects of nonlocal character are significant. In other words, the damage at a point is influenced by the damage of the neighboring points. Starting from the integral form of the nonlocal theory (Pijaudier-Cabot and Bazant, 1987; Bazant and Pijaudier-Cabot, 1988), one can show by adopting some simplified assumptions that a nonlocal variable can be expressed in terms of its local part and the corresponding Laplacian

(i.e., second-order gradient) (see e.g., de Borst and Mühlhaus, 1992; Voyiadjis and Dorgan, 2001; Voyiadjis et al., 2003, 2004; Abu Al-Rub and Voyiadjis, 2006; and the references quoted therein) such that $\widehat{\varphi}_{ij}^{\pm}$ can be expressed by:

$$\widehat{\varphi}_{ij}^{\pm} = \widehat{\varphi}_{ij}^{\pm} + \ell^{\pm 2}\nabla^2\widehat{\varphi}_{ij}^{\pm} \tag{23}$$

where $\varphi_{ij}^{\pm}$ is the local damage tensor, $\nabla^2\varphi_{ij}^{\pm}$ is the Laplacian of the damage tensors, and $\ell^{\pm}$ is the material length scale parameter. Hereafter, the superimposed hat ($\widehat{\bullet}$) designates a nonlocal quantity, and $\nabla^2\bullet = \partial^2\bullet/\partial x^2 + \partial^2\bullet/\partial y^2 + \partial^2\bullet/\partial z^2$ where x, y, and z are the rectangular Cartesian coordinates. In brittle materials the material length scale can be related to the width of the fracture process zone; in crystalline materials it can be related to the grain size or spacing between dislocations; in composite materials it can be related to the size of inclusions (or particles) (see Abu Al-Rub (2004) for more details on the physical interpretation of the material length scale). For concrete the localized damage behavior is very different in tension and compression, and therefore it seems reasonable to introduce two different material length scales, ℓ^{+} and ℓ^{-}, one for prevailing tensile damage states and the other for prevailing compressive damage states, to take into account such difference in tensile and compressive damage behavior. Similar arguments have been presented by Comi (2001), where two different weighting functions in the nonlocal integral approach have been assumed in order to characterize the different behavior in tension and compression for concrete-like materials.

The nonlocal gradient-enhanced model is then obtained by replacing the local variables $\varphi_{ij}^{\pm}$, M_{ijkl}, and $\omega^{\pm}$ in the damage evolution equations, Equations (16), (17), (20), and (21), by their corresponding nonlocal parts $\widehat{\varphi}_{ij}^{\pm}$, $\widehat{M}_{ijkl}$, and $\widehat{\omega}^{\pm}$, respectively. However, coupled terms will be obtained between $\varphi_{ij}^{\pm}$, the local damage tensor, and $\nabla^2\varphi_{ij}^{\pm}$ the Laplacian of the damage tensor. In order to avoid such mixing of the terms between the local and Laplacian terms a similar expression to Equation (23) for $\hat{\omega}^{\pm}$ is postulated. This is equivalent to the rate of the nonlocal damage variable, $\dot{\widehat{\varphi}}_{ij}^{\pm}$, such that the rate of the nonlocal equivalent damage, $\dot{\widehat{\omega}}^{\pm}$, is now expressed as follows:

$$\dot{\widehat{\omega}}^{\pm} = \dot{\omega}^{\pm} + \ell^{\pm 2}\nabla^2\dot{\omega}^{\pm} \tag{24}$$

The nonlocal model is thus completed by the loading–unloading conditions in Equation (19) in which $g^{\pm}$ are replaced by the nonlocal-enhanced parts.

Therefore, only the inelastic behavior involving damage evolution is treated as nonlocal, while the elastic and effective (undamaged) plastic constitutive relations remain local. This satisfies the requirement stated by Pijaudier-Cabot and Bazant (1987) that nonlocality in damage models can be introduced either by a nonlocal damage variable (i.e., $\tilde{\varphi}_{ij}^{\pm} = \varphi_{ij}^{\pm} + \ell^{\pm 2}\nabla^2\varphi_{ij}^{\pm}$) or a nonlocal damage force (i.e., $\tilde{Y}_{ij}^{\pm} = Y_{ij}^{\pm} + \ell^{\pm 2}\nabla^2 Y_{ij}^{\pm}$). Accordingly, the activation of tensile damage is modified by the existence of a tensile intrinsic length scale, ℓ^{+}, and the activation of compressive damage is modified by the existence of a compressive intrinsic length scale, ℓ^{-}. Furthermore, a rigorous thermodynamic formulation of the proposed model can be obtained following the same lines proposed by Voyiadjis et al. (2001, 2003, 2004) and Abu Al-Rub and Voyiadjis (2006).

Spectral Decomposition

Concrete has distinct behavior in tension and compression. Therefore, in order to adequately characterize the damage in concrete due to tensile and compressive loading conditions, the Cauchy stress tensor (nominal or effective) can be decomposed into a positive and negative parts using the spectral decomposition technique (see e.g., Ortiz, 1985; Ju, 1989; Lubarda et al., 1994; Krajcinovic, 1996). Therefore, the effective stress, $\bar{\sigma}_{ij}$, can be decomposed as follows:

$$\bar{\sigma}_{ij} = \bar{\sigma}_{ij}^{+} + \bar{\sigma}_{ij}^{-} \tag{25}$$

where $\bar{\sigma}_{ij}^{+}$ is the tensile part and $\bar{\sigma}_{ij}^{-}$ is the compressive part of the effective stress tensor.

The stress tensors $\bar{\sigma}_{ij}^{+}$ and $\bar{\sigma}_{ij}^{-}$ can be related to $\bar{\sigma}_{ij}$ by:

$$\bar{\sigma}_{kl}^{+} = P_{klpq}^{+}\bar{\sigma}_{pq}, \quad \bar{\sigma}_{kl}^{-} = \left[I_{klpq} - P_{ijpq}^{+}\right]\sigma_{pq} = P_{klpq}^{-}\bar{\sigma}_{pq} \tag{26}$$

such that $P_{ijkl}^{+} + P_{ijkl}^{-} = I_{ijkl}$. The fourth-order projection tensors P_{ijkl}^{+} and P_{ijkl}^{-} are defined as follows:

$$P_{ijpq}^{+} = \sum_{k=1}^{3} H(\hat{\bar{\sigma}}^{(k)}) n_i^{(k)} n_j^{(k)} n_p^{(k)} n_q^{(k)}, \quad P_{klpq}^{-} = I_{klpq} - P_{ijpq}^{+} \tag{27}$$

where $H(\hat{\bar{\sigma}}^{(k)})$ denotes the Heaviside step function computed at k-th principal stress $\hat{\bar{\sigma}}^{(k)}$ of $\bar{\sigma}_{ij}$, and $n_i^{(k)}$ is the k-th corresponding unit principal direction.

Similar to the decomposition of $\bar{\sigma}_{ij}$ into tensile and compressive parts, Equation (25), one can decompose σ_{ij} as follows:

$$\sigma_{ij} = \sigma_{ij}^{+} + \sigma_{ij}^{-} \tag{28}$$

Based on the above decomposition, one can assume that the expression in Equation (22) to be valid for both tension and compression separately such that:

$$\sigma_{ij}^{+} = \left(\widehat{M}_{ijkl}^{+}\right)^{-1} \bar{\sigma}_{kl}^{+}, \quad \sigma_{ij}^{-} = \left(\widehat{M}_{ijkl}^{-}\right)^{-1} \bar{\sigma}_{kl}^{-} \tag{29}$$

where $\widehat{M}_{ijkl}^{+}$ is the nonlocal tensile damage-effect tensor and $\widehat{M}_{ijkl}^{-}$ is the corresponding nonlocal compressive damage-effect tensor. The superscript $(\,)^{-1}$ indicates the inverse.

In this article, the nonlocal form of $(\widehat{M}_{ijkl})^{-1}$ that has been proposed by Voyiadjis et al. (2004) and Abu Al-Rub and Voyiadjis (2006) will be generalized to tensile and compressive damages, $\widehat{\varphi}_{ij}^{+}$ and $\widehat{\varphi}_{ij}^{-}$, as follows:

$$\begin{aligned}
\left(M_{ijkl}^{+}\right)^{-1} &= \frac{1}{2}\left[(\delta_{ij} - \widehat{\varphi}_{ij}^{+})\delta_{kl} + \delta_{ij}(\delta_{kl} - \widehat{\varphi}_{kl}^{+})\right], \\
\left(M_{ijkl}^{-}\right)^{-1} &= \frac{1}{2}\left[(\delta_{ij} - \widehat{\varphi}_{ij}^{-})\delta_{kl} + \delta_{ij}(\delta_{kl} - \widehat{\varphi}_{kl}^{-})\right]
\end{aligned} \tag{30}$$

Now, by substituting Equation (29) into Equation (28) along Equation (26), one can express the nominal stress tensor as follows:

$$\sigma_{ij} = \left[\left(\widehat{M}_{ijkl}^{+}\right)^{-1} P_{klpq}^{+} + \left(\widehat{M}_{ijkl}^{-}\right)^{-1} P_{klpq}^{-}\right] \bar{\sigma}_{pq} \tag{31}$$

By comparing the result in Equation (31) with Equation (22), one can obtain the following relation for the inverse of the total nonlocal damage-effect tensor:

$$\left(\widehat{M}_{ijpq}\right)^{-1} = \left(\widehat{M}_{ijkl}^{+}\right)^{-1} P_{klpq}^{+} + \left(\widehat{M}_{ijkl}^{-}\right)^{-1} P_{klpq}^{-} \tag{32}$$

Using Equation $(27)_2$, the above equation can be rewritten as follows:

$$\left(\widehat{M}_{ijpq}\right)^{-1} = \left[\left(\widehat{M}_{ijkl}^{+}\right)^{-1} - \left(\widehat{M}_{ijkl}^{-}\right)^{-1}\right] P_{klpq}^{+} + \left(\widehat{M}_{ijpq}^{-}\right)^{-1} \tag{33}$$

This expression implies that the compressive damage affects the tensile damage, which allows modeling the decrease of the load-carrying capacity in tension due to compressive damage and vice versa.

It is noteworthy that if the projection tensors, P^{+}_{ijkl} and P^{-}_{ijkl}, that defines the spectral decomposition of $\bar{\sigma}_{ij}$ in Equations (26) and (27) are the same for the decomposition of σ_{ij}, then by repeating the above procedure used in obtaining Equation (32) one can express the nonlocal form of the damage-effect tensor as:

$$\widehat{M}_{ijpq} = \left(\widehat{M}^{+}_{ijkl} - \widehat{M}^{-}_{ijkl}\right) P^{+}_{klpq} + \widehat{M}^{-}_{ijpq} \tag{34}$$

which implies that the inverse of Equation (33) yields Equation (34) providing that the unit principle directions, $n^{(k)}_{i}$ ($k = 1,2,3$), of both $\bar{\sigma}_{ij}$ and σ_{ij} are the same.

Moreover, it is noteworthy that if an isotropic (scalar) damage formulation is adapted with two scalar damage parameters $\widehat{\varphi}^{+}$ and $\widehat{\varphi}^{-}$ are introduced, one can simply show that damage anisotropy is still enhanced through the spectral projection tensors such that Equation (32) is reduced to:

$$\widehat{M}^{-1}_{ijkl} = (1 - \widehat{\varphi}^{+}) P^{+}_{ijkl} + (1 - \widehat{\varphi}^{-}) P^{-}_{ijkl} \tag{35}$$

However, it is anticipated that this anisotropy is weak as compared to the anisotropic damage enhanced through Equation (32). This important note will be further investigated in the future by the current authors since it decides whether the two scalar damage variables, one for tension and the other for compression, are enough for describing the damage anisotropy in concrete-like materials.

NUMERICAL INTEGRATION OF THE CONSTITUTIVE MODEL

In this section, the time descretization and numerical integration procedures of the gradient-enhanced plastic-damage model are presented. The evolutions of the plastic and damage internal state variables can be obtained if the Lagrangian multipliers $\dot{\lambda}^{\mathrm{p}}$ and $\dot{\lambda}^{\pm}_{\mathrm{d}}$ are computed. The plasticity and damage consistency conditions, Equations (14) and (19), are used for computing both $\dot{\lambda}^{\mathrm{p}}$ and $\dot{\lambda}^{\pm}_{\mathrm{d}}$. This is shown in the subsequent developments. Then, by applying the given strain increment $\Delta\varepsilon_{ij} = \varepsilon^{(n+1)}_{ij} - \varepsilon^{(n)}_{ij}$, where Δ indicates the increment of a variable over the step, and knowing the values of the stress and internal variables at the beginning of the step from the previous step, $(\,)^{(n)}$, the updated values at the end of the step, $(\,)^{(n+1)}$, are obtained.

Due to the (a) adoption of the strain equivalence hypothesis and (b) the description of plasticity constitutive relations in the effective configuration, one can easily split the numerical integration task into a decoupled plastic and nonlocal-damage return mapping algorithm. This is numerically attractive since it eliminates any computational complexity that arises from coupled equations. Therefore, the implemented integration scheme is divided into two sequential steps, corresponding to the plastic and damage parts of the model. In the plastic part, the plastic strain $\varepsilon_{ij}^{\mathrm{p}}$ and the effective stress $\bar{\sigma}_{ij}$ at the end of the step are determined by using the classical radial return mapping algorithm (Simo and Hughes, 1998). In the damage part, the nominal stress σ_{ij} at the end of the step is obtained from Equation (31) by knowing the damage variables $\varphi_{ij}^{\pm}$ and $\omega^{\pm}$ and their corresponding second-order gradients, $\nabla^2\varphi_{ij}^{\pm}$ and $\nabla^2\omega^{\pm}$, respectively, which can be calculated once $\Delta\lambda_{\mathrm{d}}^{\pm}$ is computed from the damage consistency condition as will be shown in the subsequent sections.

Elastic Predictor

The elastic predictor can be tentatively obtained by assuming the entire strain increment $\Delta\varepsilon$ as elastic, such that

$$\bar{\sigma}_{ij}^{\mathrm{tr}} = \bar{\sigma}_{ij}^{(n)} + \bar{E}_{ijkl}\Delta\varepsilon_{kl} \tag{36}$$

For this tentative stress state, the trial plastic function is given by:

$$f^{\mathrm{tr}} = \sqrt{\frac{3}{2}}\left\|\bar{s}_{ij}^{\mathrm{tr}}\right\| + \alpha\bar{I}_1^{\mathrm{tr}} - \bar{\beta}\hat{\bar{\sigma}}_{\max}^{\mathrm{tr}} - (1-\alpha)c^{-(n)} \tag{37}$$

where $\bar{s}_{ij}^{\mathrm{tr}} = \bar{\sigma}_{ij}^{\mathrm{tr}} - (1/3)\bar{\sigma}_{kk}^{\mathrm{tr}}\delta_{ij}$. If $f^{\mathrm{tr}} \leq 0$, plasticity does not occur in this step, and then $\bar{\sigma}_{ij}^{\mathrm{tr}}$ is accepted as $\bar{\sigma}_{ij}^{(n+1)}$ and one sets $\Delta\lambda^{\mathrm{p}} = 0$, $\varepsilon_{ij}^{\mathrm{p}(n+1)} = \varepsilon_{ij}^{\mathrm{p}(n)}$, and $c^{\pm(n+1)} = c^{\pm(n)}$. This means that the response is elastic in the effective (undamaged) configuration and the damage corrector should then be applied.

Plastic Corrector

If $f^{\mathrm{tr}} > 0$, $\bar{\sigma}_{ij}^{\mathrm{tr}}$ cannot be accepted as $\bar{\sigma}_{ij}^{(n+1)}$ due to plasticity. Then $\bar{\sigma}_{ij}^{(n+1)}$ can be written using Equations (4), (5), (13), (15), and (36) as follows:

$$\bar{\sigma}_{ij}^{(n+1)} = \bar{\sigma}_{ij}^{\mathrm{tr}} - \bar{E}_{ijkl}\Delta\varepsilon_{kl}^{\mathrm{p}} = \bar{\sigma}_{ij}^{\mathrm{tr}} - \Delta\lambda^{\mathrm{p}}\left[\sqrt{6}\bar{G}\frac{\bar{s}_{ij}^{(n+1)}}{\left\|\bar{s}_{ij}^{(n+1)}\right\|} + 3\bar{K}\alpha^{\mathrm{p}}\delta_{ij}\right] \tag{38}$$

where $-\bar{E}_{ijkl}\Delta\varepsilon_{kl}^{\mathrm{p}}$ is the plastic corrector.

One can simply show that Equation (38) can be written for the principal stress $\hat{\bar{\sigma}}_{\max}$ as follows:

$$\hat{\bar{\sigma}}_{\max}^{(n+1)} = \hat{\bar{\sigma}}_{\max}^{\mathrm{tr}} - \Delta\lambda^{\mathrm{p}}\left[\sqrt{6}\bar{G}\frac{\hat{\bar{\sigma}}_{\max}^{(n+1)}}{\left\|\bar{s}_{ij}^{(n+1)}\right\|} + 3\bar{K}\alpha^{\mathrm{p}} - \sqrt{\frac{2}{3}}\bar{G}\frac{\bar{I}_1^{(n+1)}}{\left\|\bar{s}_{ij}^{(n+1)}\right\|}\right] \tag{39}$$

Then $\bar{\sigma}_{ij}^{(n+1)}$, $\varepsilon_{ij}^{\mathrm{p}(n+1)}$, and $c^{\pm(n+1)}$ can be determined by computing $\Delta\lambda^{\mathrm{p}}$ using the plasticity consistency condition, Equation $(14)_4$:

$$\Delta f = \frac{\partial f}{\partial \bar{\sigma}_{ij}}\Delta\bar{\sigma}_{ij} + \frac{\partial f}{\partial \hat{\bar{\sigma}}_{\max}}\Delta\hat{\bar{\sigma}}_{\max} + \frac{\partial f}{\partial \kappa^-}\Delta\kappa^- + \frac{\partial f}{\partial \kappa^+}\Delta\kappa^+ = 0 \tag{40}$$

In order to return radially to the yield surface, one can use the radial return algorithm assumption (Simo and Hughes, 1998) such that:

$$\frac{\bar{s}_{ij}^{(n+1)}}{\left\|\bar{s}_{ij}^{(n+1)}\right\|} = \frac{\bar{s}_{ij}^{\mathrm{tr}}}{\left\|\bar{s}_{ij}^{\mathrm{tr}}\right\|} \tag{41}$$

Substituting the increments of Equations (38) and (39) along with Equation (10), one can obtain the plastic multiplier $\Delta\lambda^{\mathrm{p}}$ from the following expression:

$$\Delta\lambda^{\mathrm{p}} = \frac{f^{\mathrm{tr}}}{H} \tag{42}$$

where H is given by

$$H = 3\bar{G} + 9\bar{K}\alpha^{\mathrm{p}}\alpha + \beta^{\mathrm{tr}}H(\hat{\bar{\sigma}}_{\max}^{\mathrm{tr}})Z + (1-r)\frac{\partial f}{\partial \kappa^-}\frac{\partial F^{\mathrm{p}}}{\partial \hat{\bar{\sigma}}_{\min}^{\mathrm{tr}}} - r\frac{\partial f}{\partial \kappa^+}\frac{\partial F^{\mathrm{p}}}{\partial \hat{\bar{\sigma}}_{\max}^{\mathrm{tr}}} \tag{43}$$

with

$$Z = \sqrt{6}\bar{G}\frac{\hat{\bar{\sigma}}_{\max}^{\mathrm{tr}}}{\left\|\bar{s}_{ij}^{\mathrm{tr}}\right\|} + 3\bar{K}\alpha^{\mathrm{p}} - \sqrt{\frac{2}{3}}\bar{G}\frac{\bar{I}_1^{\mathrm{tr}}}{\left\|\bar{s}_{ij}^{\mathrm{tr}}\right\|} \tag{44}$$

$$\frac{\partial F^{\mathrm{p}}}{\partial \hat{\bar{\sigma}}_{\min,\max}^{\mathrm{tr}}} = \sqrt{\frac{3}{2}}\frac{(\hat{\bar{\sigma}}_{\min,\max}^{\mathrm{tr}} - \frac{1}{3}\bar{I}_1^{\mathrm{tr}})}{\left\|\bar{s}_{ij}^{\mathrm{tr}}\right\|} + \alpha^{\mathrm{p}} \tag{45}$$

$$\frac{\partial f}{\partial \kappa^-} = -(1-\alpha)Qb\exp(-b\kappa^-)\left[1 - \frac{\langle \hat{\bar{\sigma}}_{\max}\rangle}{c^+}\right] \tag{46}$$

$$\frac{\partial f}{\partial \kappa^+} = -\langle \hat{\bar{\sigma}}_{\max}\rangle \frac{c^-(1-\alpha)h}{(c^+)^2} \tag{47}$$

Both $\partial f/\partial\kappa^+$ and $\partial f/\partial\kappa^-$ are calculated by substituting the values from the previous step. Once $\Delta\lambda^{\mathrm{p}}$ is calculated from Equations (37) and (42)–(47), one can then calculate the effective stress $\bar{\sigma}_{ij}^{(n+1)}$ from Equations (38) and (41). The next step is checking the damage nucleation and growth conditions, Equation (19), and calculating the final nominal stress $\sigma_{ij}^{(n+1)}$.

Damage Corrector

Now, one can check the damage nucleation and growth conditions by substituting the updated effective stress from the plastic corrector step, $\bar{\sigma}_{ij}^{(n+1)}$, and the values of $\widehat{\varphi}_{ij}^{\pm}$ and $K^{\pm}$ from the previous step (i.e., at n time step) into Equations (16), (20), and (21). If $g^{\pm} \leq 0$, then the final nominal stress is set equal to the effective stress obtained from the plasticity corrector step (i.e., $\sigma_{ij}^{(n+1)} = \bar{\sigma}_{ij}^{(n+1)}$). Whereas, if one or both of $g^+ > 0$ and $g^+ > 0$ are satisfied, then one should proceed with the damage corrector step in order to calculate the nonlocal damage variables, $\widehat{\varphi}_{ij}^{\pm}$ and $\widehat{\omega}^{\pm}$, in Equation (23) such that one can update the final nominal stress as:

$$\sigma_{ij}^{(n+1)} = \left(\widehat{M}_{ijkl}^{(n+1)}\right)^{-1} \bar{\sigma}_{kl}^{(n+1)} \tag{48}$$

where $\bar{\sigma}_{kl}^{(n+1)}$ is the stress field from the plastic corrector step. Therefore, in order to accomplish this step, the damage multiplier $\Delta\lambda_{\mathrm{d}}^{\pm}$ needs to be calculated first using the consistency condition in Equation (19). In the following the tensile damage and compressive damage consistency conditions will be used in a unified way such that $\pm$ indicates either tension or compression. The incremental expression for the damage consistency condition can be written as:

$$\Delta g^{\pm} = \frac{\partial g^{\pm}}{\partial Y_{ij}^{\pm}} \Delta Y_{ij}^{\pm} + \frac{\partial g^{\pm}}{\partial K^{\pm}} \Delta K^{\pm} = 0 \tag{49}$$

However, it can be noted from Equation (21) that the damage force $Y_{ij}^{\pm}$ is a function of $\sigma_{ij}^{\pm}$ and $\widehat{\varphi}_{ij}^{\pm}$ such that one can write the following:

$$\Delta Y_{ij}^{\pm} = \frac{\partial Y_{ij}^{\pm}}{\partial \sigma_{kl}^{\pm}} \Delta\sigma_{kl}^{\pm} + \frac{\partial Y_{ij}^{\pm}}{\partial \widehat{\varphi}_{kl}^{\pm}} \Delta\widehat{\varphi}_{kl}^{\pm} \tag{50}$$

One can then rewrite Equation (49) as follows:

$$\Delta g^{\pm} = \frac{\partial g^{\pm}}{\partial \sigma_{kl}^{\pm}} \Delta \sigma_{kl}^{\pm} + \frac{\partial g^{\pm}}{\partial \widehat{\varphi}_{kl}^{\pm}} \Delta \widehat{\varphi}_{kl}^{\pm} - \aleph^{\pm} \Delta \widehat{\omega}^{\pm} = 0 \tag{51}$$

where $\partial g^{\pm}/\partial K^{\pm} = -1$ is used in writing the above equation by substituting Equation (16), and the expressions for $\aleph^{+}$ and $\aleph^{-}$ are given from Equation (20) as follows:

$$\aleph^{+} = \frac{K^{+}}{B^{+} + (K_0^{+}/K^{+})} \exp\left[-B^{+}\left(1 - \frac{K^{+}}{K_0^{+}}\right)\right], \quad \aleph^{-} = \frac{K_0^{-}}{B^{-}} \exp\left[-B^{-}\left(1 - \frac{K^{-}}{K_0^{-}}\right)\right] \tag{52}$$

In order to simplify the presentation of the derived equations, the superscript $\pm$ is dropped from the following development. Therefore, for each quantity in the subsequent equations there is a tensile part and a compressive part.

An expression for $\Delta \sigma_{kl}$ can be obtained from Equation (29) as follows:

$$\Delta \sigma_{kl} = \frac{\partial \widehat{M}_{klrs}^{-1}}{\partial \widehat{\varphi}_{mn}} \Delta \widehat{\varphi}_{mn} \bar{\sigma}_{rs} + \widehat{M}_{klrs}^{-1} \Delta \bar{\sigma}_{rs} \tag{53}$$

Substituting Equation (18) into Equation (23) and writing the result in an increment format yields:

$$\Delta \widehat{\varphi}_{kl} = \left(\Delta \lambda_{\mathrm{d}} + \ell^2 \nabla^2 \Delta \lambda_{\mathrm{d}}\right) \frac{\partial g}{\partial Y_{kl}} + 2\ell^2 (\Delta \lambda_{\mathrm{d}})_{,m} \left(\frac{\partial g}{\partial Y_{kl}}\right)_{,m} + \Delta \lambda_{\mathrm{d}} \ell^2 \nabla^2 \left(\frac{\partial g}{\partial Y_{kl}}\right) \tag{54}$$

where $(\bullet)_{,m}$ designates the first derivative of $(\bullet)$ with respect to x_m. However, one can assume that the unit normal to the damage surface, $\partial g/\partial Y_{ij}$, is the same at every point within the localized damage zone such that the first- and second-order gradients of $\partial g/\partial Y_{ij}$ are zero. By employing this assumption, the last two terms drop from Equation (54) such that one can write:

$$\Delta \widehat{\varphi}_{kl} = \left(\Delta \lambda_{\mathrm{d}} + \ell^2 \nabla^2 \Delta \lambda_{\mathrm{d}}\right) \frac{\partial g}{\partial Y_{kl}} \tag{55}$$

Substituting Equations (24) and (53) into Equation (51) and making use of Equation (55) and recalling that $\Delta \omega = \Delta \lambda_{\mathrm{d}}$, one obtains the following expression:

$$g^{\mathrm{tr}} + V\left(\Delta \lambda_{\mathrm{d}} + \ell^2 \nabla^2 \Delta \lambda_{\mathrm{d}}\right) = 0 \tag{56}$$

where g^{tr} is the trial value of the damage surface, which is obtained by substituting the values of $Y_{ij}^{\mathrm{tr}}\left(\bar{\sigma}_{ij}^{(n+1)}, \widehat{\varphi}_{ij}^{(n)}\right)$ and $K^{(n)}$ in Equation (16). The scalar V in Equation (56), which is calculated by substituting the values from the previous step, is given by:

$$V = \left[\frac{\partial g}{\partial \sigma_{mn}} \frac{\partial \widehat{M}^{-1}_{mnpq}}{\partial \widehat{\varphi}_{rs}} \bar{\sigma}_{pq} + \frac{\partial g}{\partial \widehat{\varphi}_{rs}}\right] \frac{\partial g}{\partial Y_{rs}} - \aleph \tag{57}$$

The expressions for $\partial g/\partial Y_{rs}$, $\partial \widehat{M}^{-1}_{mnpq}/\partial \widehat{\varphi}_{rs}$, $\partial g/\partial \sigma_{mn}$, and $\partial g/\partial \widehat{\varphi}_{rs}$ can be obtained by making use of Equations (16), (21), (22), and (30) along with the identity $\widehat{M}_{ijab}\widehat{M}^{-1}_{abkl} = I_{ijkl}$ as follows:

$$\frac{\partial g}{\partial Y_{rs}} \equiv \frac{L_{rskl} Y_{kl}}{\sqrt{2\, Y_{mn} L_{mnpq} Y_{pq}}} \tag{58}$$

$$\frac{\partial \widehat{M}^{-1}_{mnpq}}{\partial \widehat{\phi}_{rs}} = -\frac{1}{2}\left(\delta_{mn}\delta_{ps}\delta_{qs} + \delta_{pq}\delta_{mr}\delta_{ns}\right) \tag{59}$$

$$\frac{\partial g}{\partial \sigma_{mn}} = \frac{\partial g}{\partial Y_{rs}} \frac{\partial Y_{rs}}{\partial \sigma_{mn}} = \frac{\partial g}{\partial Y_{rs}} \left[-\bar{E}^{-1}_{klab} \bar{\sigma}_{ab} \frac{\partial \widehat{M}^{-1}_{klpq}}{\partial \widehat{\varphi}_{rs}} \widehat{M}_{pqmn}\right] \tag{60}$$

$$\frac{\partial g}{\partial \widehat{\phi}_{rs}} \equiv \frac{\partial g}{\partial Y_{mn}} \frac{\partial Y_{mn}}{\partial \phi_{rs}} = \frac{\partial g}{\partial Y_{mn}} \left[\bar{E}^{-1}_{uvab} \bar{\sigma}_{ab} \frac{\partial \widehat{M}^{-1}_{uvpq}}{\partial \widehat{\varphi}_{mn}} \widehat{M}_{pqkl} \frac{\partial \widehat{M}^{-1}_{klcd}}{\partial \widehat{\varphi}_{rs}} \bar{\sigma}_{cd}\right] \tag{61}$$

Due to the presence of the second-order gradient in Equation (56), $\nabla^2 \Delta\lambda_{\mathrm{d}}$, considerable difficulties are experienced with the numerical calculation of $\Delta\lambda_{\mathrm{d}}$ necessary to finish the damage corrector step. The damage consistency condition is no longer an algebraic equation but is a differential one. Another complication is the application of a higher order (nonclassical) boundary condition at the boundary of the evolving damage zone, which is necessary for the mathematical consistency of the nonlocal gradient-dependent approach (Mühlhaus and Aifantis, 1991; Pamin, 1994) such that $\Delta\lambda_{\mathrm{d}} = 0$ is prescribed at the damage zone boundary. Should the damage zone spread over the specimen boundaries, then one should apply $\partial \Delta\lambda_{\mathrm{d}}/\partial x_k = 0$ and $\nabla^2 \Delta\lambda_{\mathrm{d}} = 0$ at the specimen's damaged boundaries

(i.e., the first- and second-order gradients vanish at the damaged boundaries). The physical interpretation of the higher order boundary conditions in the gradient-dependent approach have been discussed by Gudmundson (2004) and Abu Al-Rub et al. (2007).

The computational technique that is commonly followed for integrating the gradient-enhanced constitutive relations was first proposed by de Borst and co-workers (e.g., de Borst and Mühlhaus, 1992; de Borst et al., 1993; Pamin, 1994; de Borst and Pamin, 1996; Peerlings et al., 1996; de Borst et al., 1999; Pamin et al., 2003; and the references quoted therein). In their approach, within the finite element context, the damage multiplier $\Delta\lambda_d$ is considered as an additional degree of freedom having a role similar to that of the displacement and is discretized in addition to the usual discretization of the displacement. In addition, the consistency condition is written in a weak form and solved simultaneously with the equation of motion. However, because of the presence of high-order derivatives in the weak form of the (initial) boundary value problem, there is a need for numerically expensive C^1-continuous conditions on the shape functions or penalty-enhanced C^0 class functions for the interpolation of the damage multiplier. Therefore, in the de Borst approach Hermitian or mixed formulations are unavoidable for a consistent finite element formulation and, for the inelastic process, a standard return mapping algorithm is performed in which the values of the kinematic fields at an integration point are interpolated from their nodal values. This approach has been discussed thoroughly by Voyiadjis et al. (2001, 2004) and used intensively by many other authors (e.g., Comi and Perego, 1996; Mikkelsen, 1997; Ramaswamy and Aravas, 1998a, b; Svedberg and Runesson, 2000; Zervos et al., 2001; Nedjar, 2001; Matsushima et al., 2002; Chen and Yuan, 2002; Liebe et al., 2003; and the references quoted therein). The disadvantage of this approach is that it gives rise to many numerical difficulties that require considerable modifications to the existing finite element codes, which makes their implementation not an easy or a direct task.

Abu Al-Rub and Voyiadjis (2005) have proposed an alternative approach for the gradient-dependent constitutive models, which can be implemented in the existing finite element codes without numerous modifications as compared to the de Borst approach such that neither the damage multiplier is introduced as an additional degree of freedom nor high-order continuous shape functions (e.g., C^1 class or penalty-enhanced C^0 class functions) are needed for the interpolation of the damage multiplier in the finite element context. In consequence, a straightforward one-field C^0-continuous finite element implementation can be easily used. Furthermore, this algorithm has the major advantage that it avoids boundary conditions on the moving damage zone boundary since the resulting partial deferential equations hold

over the whole body. Voyiadjis and Abu Al-Rub (2006) have adopted this approach for more complex problems involving a projectile moving with hyper-velocities and penetrating a target. They could use directly the already available contact elements in the commercial finite element code ABAQUS (2003) to model the contact process; unlike if one adapts the de Borst approach where new contact elements should be implemented. In the following section, this approach is adapted for computing $\nabla^2\Delta\lambda_d$ that appears in Equation (56) at each integration point.

Computation of the Laplacian of the Damage Multipliers

In the approach proposed by Abu Al-Rub and Voyiadjis (2005) the nonlocal damage consistency condition, Equation (56), can be transformed into a linear set of equations that depends on the material parameters and on the current coordinates of the integration points. These sets of linear equations are then solved by any numerical iterative method (e.g., Gauss–Jordan method) for the damage multipliers at all integration points. The Laplacian of the damage multiplier, $\nabla^2\Delta\lambda_d$, at each integration point m is computed from the derivatives of a polynomial function that interpolates the value of the damage multiplier, $\Delta\lambda_d$, at the neighboring points. This procedure enforces the consistency condition, Equation (56), in the sense of distributions, i.e., the damage condition $g=0$ is satisfied at the end of the loading step. Therefore, in order to compute the Laplacian $\nabla^2\Delta\lambda_d$ at an integration point m, one needs the values of $\Delta\lambda_d$ at point m as well as at the neighboring points (nonlocality) such that $\nabla^2\Delta\lambda_d^{(m)}$ can be expressed in terms of $\Delta\lambda_d^{(k)}$ with $k \in \{1,\ldots,N\text{GP}\}$ using the least-squares method:

$$\nabla^2\Delta\lambda_d^{(m)} = \sum_{k=1}^{N_{GP}} \Omega^{(mk)}\Delta\lambda_d^{(k)} \tag{62}$$

where N_{GP} is the number of Gauss integration points and $\Omega^{(mk)}$ is a coefficient matrix that can be computed for 2D problems by assuming a polynomial function for $\Delta\lambda_d$ around point m, such that:

$$\Delta\lambda_d = \mathbf{a}^T\mathbf{v} \tag{63}$$

where $\mathbf{a}$ is the coefficients vector, and $\mathbf{v}$ is the variables vector. For example in a 2D setting, the expressions for $\mathbf{a}$ and $\mathbf{v}$ are: $\mathbf{a}^T = \lfloor a_1 \;\; a_2 \;\; a_3 \;\; a_4 \;\; a_5 \;\; a_6 \rfloor$ and $\mathbf{v}^T = \lfloor 1 \;\; x \;\; y \;\; xy \;\; x^2 \;\; y^2 \rfloor$. In this section, we shifted to matrix notation to simplify the presentation of the derived equations where the superscript $(\bullet)^T$ designates the transpose of a vector or a matrix.

In order to obtain the coefficients vector **a**, a minimization method by least squares is used. Moreover, the interpolation is made in the global coordinate system (x,y,z) of the generated mesh with N_{GP} integration points. The coefficients vector **a** can be expressed in the following form:

$$\mathbf{\Lambda} = \mathbf{W}^T \mathbf{a} \tag{64}$$

where $\mathbf{\Lambda} = \begin{bmatrix} \Delta\lambda_d^{(1)} & \Delta\lambda_d^{(2)} & \cdots & \Delta\lambda_d^{(N_{GP})} \end{bmatrix}^T$. For a 2D mesh the matrix **W** is defined by:

$$\mathbf{W} = \left[\mathbf{v}^{(1)}\mathbf{v}^{(2)}\cdots\mathbf{v}^{(N_{GP})}\right] = \begin{bmatrix} 1 & 1 & \cdots & 1 \\ x_1 & x_2 & \cdots & x_{N_{GP}} \\ y_1 & y_2 & \cdots & y_{N_{GP}} \\ x_1y_1 & x_2y_2 & \cdots & x_{N_{GP}}y_{N_{GP}} \\ x_1^2 & x_2^2 & \cdots & x_{N_{GP}}^2 \\ y_1^2 & y_2^2 & \cdots & y_{N_{GP}}^2 \end{bmatrix} \tag{65}$$

where $\mathbf{v}^{(k)} = \begin{bmatrix} 1 & x_k & y_k & x_ky_k & x_k^2 & y_k^2 \end{bmatrix}^T$.

Multiplying both sides of Equation (64) by **W**, one can write:

$$\mathbf{W\Lambda} = \mathbf{Ha} \tag{66}$$

with $H = \mathbf{WW}^T$ is a symmetrical square matrix and can be written for 2D problems as:

$$\mathbf{H} = \sum_{k=1}^{N_{GP}} \mathbf{v}^{(k)}(\mathbf{v}^{(k)})^T = \sum_{k=1}^{N_{GP}} \begin{bmatrix} 1 & x_k & y_k & x_ky_k & x_k^2 & y_k^2 \\ & x_k^2 & x_ky_k & x_k^2y_k & x_k^3 & x_ky_k^2 \\ & & y_k^2 & x_ky_k^2 & x_k^2y_k & y_k^3 \\ & & & x_k^2y_k^2 & x_k^3y_k & x_ky_k^3 \\ & \text{Symm} & & & x_k^4 & x_k^2y_k^2 \\ & & & & & y_k^4 \end{bmatrix} \tag{67}$$

It is obvious that **H** needs to be updated at each loading increment for finite deformation problems.

Noticing that $\mathbf{W\Lambda}$ can be expressed as:

$$\mathbf{W\Lambda} = \sum_{k=1}^{N_{GP}} \Delta\lambda_d^{(k)} \mathbf{v}^{(k)} \tag{68}$$

one can then compute the damage multiplier and its Laplacian from Equations (63) and (66) as follows:

$$\Delta\lambda_{\mathrm{d}} = \mathbf{a}^T\mathbf{v} = \left(\mathbf{H}^{-1}\mathbf{W}\boldsymbol{\Lambda}\right)^T\mathbf{v} = \left(\mathbf{H}^{-1}\sum_{k=1}^{N_{\mathrm{GP}}}\Delta\lambda_{\mathrm{d}}^{(k)}\mathbf{v}^{(k)}\right)^T\mathbf{v} \tag{69}$$

$$\nabla^2\Delta\lambda_{\mathrm{d}} = \left(H^{-1}\sum_{k=1}^{N_{\mathrm{GP}}}\Delta\lambda_{\mathrm{d}}^{(k)}\mathbf{v}^{(k)}\right)^T\nabla^2\mathbf{v} \tag{70}$$

where $\nabla^2\mathbf{v} = \partial^2\mathbf{v}/\partial x^2 + \partial^2\mathbf{v}/\partial y^2$.

For the integration point m, one can write 2D expressions for

$$\nabla^2\Delta\lambda_{\mathrm{d}}^{(m)} = \frac{\partial^2\Delta\lambda_{\mathrm{d}}^{(m)}}{\partial x^2} + \frac{\partial^2\Delta\lambda_{\mathrm{d}}^{(m)}}{\partial y^2} \tag{71}$$

as follows

$$\nabla^2\Delta\lambda_{\mathrm{d}}^{(m)} = \sum_{k=1}^{N_{\mathrm{GP}}}\left[\left(\mathbf{v}^{(k)}\right)^T\mathbf{H}^{-1}\frac{\partial^2\mathbf{v}^{(m)}}{\partial x^2} + \left(\mathbf{v}^{(k)}\right)^T\mathbf{H}^{-1}\frac{\partial^2\mathbf{v}^{(m)}}{\partial y^2}\right]\Delta\lambda_{\mathrm{d}}^{(k)} \tag{72}$$

Comparing Equations (62) with Equation (72), one can then compute the coefficients $\Omega^{(mk)}$ using the following expression:

$$\Omega^{(mk)} = \left(\mathbf{v}^{(k)}\right)^T\mathbf{H}^{-1}\frac{\partial^2\mathbf{v}^{(m)}}{\partial x^2} + v_n^T\mathbf{H}^{-1}\frac{\partial^2 v^{(m)}}{\partial y^2} \tag{73}$$

The coefficients $\Omega^{(mk)}$ depend only on the x and y coordinates of the Gauss integration points. However, one can easily show that $\partial^2\mathbf{v}/\partial x^2 = \begin{bmatrix}0 & 0 & 0 & 0 & 2 & 0\end{bmatrix}^T$ and $\partial^2\mathbf{v}/\partial y^2 = \begin{bmatrix}0 & 0 & 0 & 0 & 0 & 2\end{bmatrix}^T$ such that one can simplify Equation (73) as follows:

$$\Omega^{(mk)} = 2\left[5\text{th Row of } \mathbf{H}^{-1} + 6\text{th Row of } \mathbf{H}^{-1}\right]\mathbf{v}^{(k)} \tag{74}$$

Using Equations (62) and (74) one can now determine nonlocally $\Delta\lambda_{\mathrm{d}}$ at each integration point m from the consistency condition in Equation (56), which is shown next.

Nonlocal Damage Corrector

In this section, the procedure for calculating the damage multiplier, $\Delta\lambda_d$, is described. Substituting Equation (62) into Equation (56), one can write at each integration point m the following:

$$g^{tr}(m) + V^{(m)}\left[\Delta\lambda_d^{(m)} + \ell^2 \sum_{k=1}^{N_{GP}} \Omega^{(mk)} \Delta\lambda_d^{(k)}\right] = 0 \tag{75}$$

where the above equation can be written as a system of linear equations as follows:

$$G\mathbf{\Lambda} = \mathbb{R} \tag{76}$$

where G and $\mathbb{R}$ are given by

$$2G = \begin{bmatrix} V^{(1)}[1+\ell^2\Omega^{(11)}] & V^{(1)}\ell^2\Omega^{(12)} & \cdots & V^{(N_{GP})}\ell^2\Omega^{(1N_{GP})} \\ V^{(2)}\ell^2\Omega^{(21)} & V^{(2)}[1+\ell^2\Omega^{(22)}] & \cdots & V^{(N_{GP})}\ell^2\Omega^{(2N_{GP})} \\ \vdots & \vdots & \ddots & \vdots \\ V^{(N_{GP})}\ell^2\Omega^{(1N_{GP})} & V^{(N_{GP})}\ell^2\Omega^{(2N_{GP})} & \cdots & V^{(N_{GP})}[1+\ell^2\Omega^{(N_{GP}N_{GP})}] \end{bmatrix} \tag{77}$$

$$\mathbb{R} = \begin{bmatrix} g^{tr(1)} & g^{tr(2)} & \cdots & g^{tr(N_{GP})} \end{bmatrix}^T \tag{78}$$

Equation (76) can be solved for Λ using a numerical iterative scheme such as the Gauss–Jordan iterative method. The damage multipliers are obtained when the damage condition, g, is fulfilled at the end of the loading step for a suitable tolerance, such that:

$$\sum_{k=1}^{N_{GP}} g^{(k)} \leq TOL \tag{79}$$

where TOL could be set to a very small value in the order of 10^{-5}.

Note that in the undamaged-elastic elements $\Delta\lambda_d^{(m)} = 0$; however, for spreading of the damage zone it is important that the numerical solution allows $\Delta\lambda_d^{(m)} > 0$ at the elastic-damage boundary. If damaged integration points appear in the structure, then in the elastic integration points adjacent to the damage zone one has nonzero $\mathbf{\Lambda}$. Therefore, the proposed algorithm has the feature, that these elastic integration points have $\Delta\lambda_d^{(m)} \approx 0$ and $\nabla^2\Delta\lambda_d^{(m)} > 0$. As a result the strength is decreased and the damage at these elastic points is delayed or enters the softening region.

Once the damage multipliers are calculated the final updated nominal stresses are calculated using Equation (48) which concludes the damage corrector step.

Finally, since the derivation of the nonlocal consistent tangent stiffness required to speed up the solution convergence is cumbersome for this model, the secant prediction stiffness in Equation (7) has been used in the numerical simulations. This choice results in a large number of iterations, but is quite efficient since it does not require the updating of the stiffness at each iteration. However, the proper definition of a nonlocal consistent tangent stiffness as proposed by Abu Al-Rub and Voyiadjis (2005) for nonlocal plasticity will be presented in the future.

NUMERICAL APPLICATIONS

In order to investigate the predictive capability and the regularization properties of the proposed model and the effectiveness of the numerical strategy, two numerical examples have been performed. The algorithmic model presented in the previous section is coded as a UMAT user material subroutine and implemented in the commercial finite element program ABAQUS (2003).

The values for $\bar{E}$, ν, f_0^+, f_0^-, α^{p}, and α are calibrated from uniaxial tension/compression tests. The damage material parameters $K_0^{\pm}$ and $B^{\pm}$ are calculated using the following relations:

$$K_0^{\pm} = \frac{f_0^{\pm 2}}{2\bar{E}}, \quad B^{\pm} = \left[\frac{G_{\mathrm{f}}^{\pm}\bar{E}}{\ell^{\pm} f_0^{\pm 2}} - \frac{1}{2}\right]^{-1} \geq 0 \tag{80}$$

where $G_{\mathrm{f}}^{\pm}$ is the fracture energy. Equation $(80)_2$ is proposed by Onate et al. (1988) where ℓ has been characterized as the size of the smallest element in a finite element mesh, which is a nonphysical length scale unlike the length scale in the present model. The experimental measure of the present length scale is far from being trivial. Comparison of experimental results in uniaxial tension/compression of concrete specimens in which damage localizes in narrow zones allows the definition of a material length scale related to the aggregate size (Bazant and Pijaudier-Cobot, 1989; Jansen and Shah, 1997). Here, the length scales ℓ^+ and ℓ^- are identified by substituting in Equation (80) the values of the tensile and compressive facture energies, G_{f}^+ and G_{f}^-, obtained from uniaxial tension/compression stress–strain diagrams after calibrating the material constants, B^+ and B^-, which give the closest fit to the experimental data.

Furthermore, it is assumed that the onset of plasticity, characterized by $f_0^{\pm}$, coincides with the onset of damage, characterized by $K_0^{\pm}$, such that

Table 1. The material constants for normal strength concrete.

$\bar{E} = 31.7\,\text{GPa}$	$\nu = 0.2$	$f_u^+ = 3.48\,\text{MPa}$	$f_u^- = 27.6\,\text{MPa}$
$f_0 + = 3.48\,\text{MPa}$	$f_0^- = 20\,\text{MPa}$	$G_f^+ = 42\,\text{N/m}$	$G_f^- = 1765\,\text{N/m}$
$\alpha^p = 0.2$	$\alpha = 0.12$	$\ell = 50\,\text{mm}$	$h = 25\,\text{GPa}$
$Q = 50\,\text{MPa}$	$b = 2200$	$B^+ = 0.54$	$B^- = 0.12$
$K_0^+ = 191\,\text{N/m}^2$	$K_0^- = 6310\,\text{N/m}^2$		

$f_0^+ = f_u^+$ whereas f_0^- is obtained beyond which nonlinearity becomes visible. Generally, h, Q, and b can be obtained by constructing the effective stress, $\bar{\sigma} = \sigma/(1 - \varphi_{11})$, versus the plastic strain diagram such that φ_{11} can be obtained by measuring the reduction in the material stiffness from loading/reloading uniaxial cyclic test (one point is extracted for each unloading cycle). However, due to the lack of such experimental data, the material constants h, Q, and b can be obtained by taking the best fit of the experimental data.

As a first example, the effectiveness of the proposed local model is demonstrated in both uniaxial and biaxial tension and compression problems and compared with experimental data (Cicekli et al., 2007). The material parameters are shown in Table 1.

It is noteworthy that without a gradient-enhanced formulation (in general without a regularization technique) the finite-element codes with strain softening exhibit unacceptable spurious mesh sensitivity. To demonstrate the capability of the present nonlocal model, the finite element simulation of two different tests in which the crack has a curved path is presented next.

Uniaxial and Biaxial Tensile/Compressive Loadings

A single-element mesh of size $200 \times 200\,\text{mm}^2$ and with one Gauss integration point is used in testing the proposed local elasto-plastic-damage model as shown in Figure 1. Simulations are performed using one step and 100 iterations. Convergence is obtained quickly. Numerical results show a good agreement between the stress–strain curves compared to the experimental results as shown for uniaxial and biaxial tensile/compressive loadings in Figures 2 and 3, respectively. Although the experimental data in Figure 2(a) show a very steep softening curve, the proposed model can predict to a large extent such a large negative stiffness. The simulated compressive stress-strain curve in Figure 2(b) agrees very well with the experimental data.

The same material constants as listed in Table 1 are used to test the model under biaxial loading. It can be seen that the dilatancy in concrete, which is

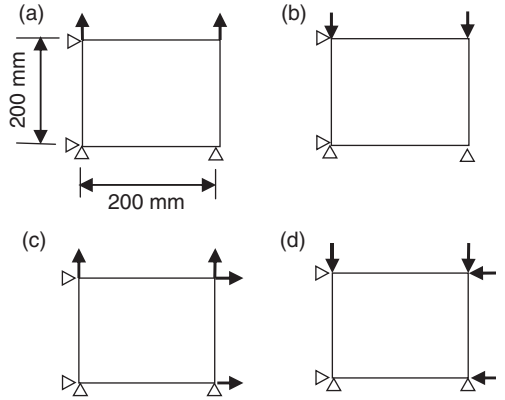

Figure 1. *(a) Uniaxial tension, (b) uniaxial compression, (c) biaxial tension, and (d) biaxial compression (Cicekli et al., 2007).*

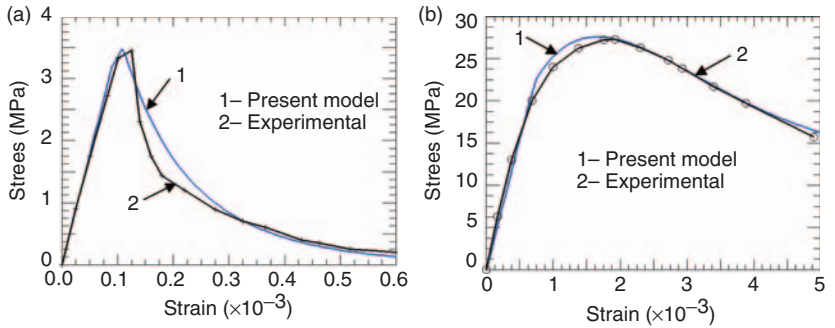

Figure 2. *Stress–strain curves for (a) uniaxial tension and (b) uniaxial compression. Comparison of the model predictions with experimental results (Karsan and Jirsa, 1969).*

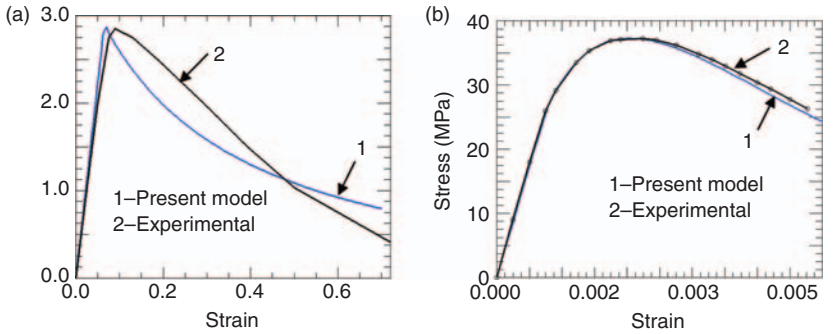

Figure 3. *Stress–strain curves for (a) biaxial tension and (b) biaxial compression. Comparison of the model predictions with experimental results (Kupfer et al., 1969).*

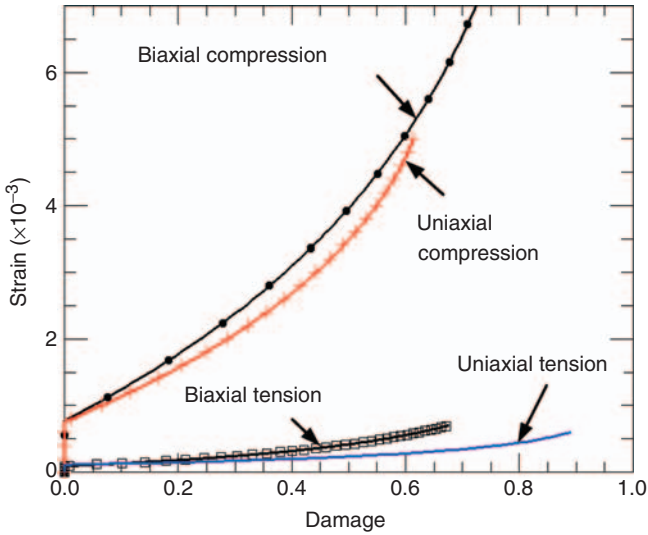

Figure 4. *Comparison between the damage evolution during uniaxial and biaxial tensile and compressive loadings.*

mainly controlled by the α^{p} parameter in the plastic potential function, can be modeled well by the present model.

Figure 4 shows the damage evolution versus strain for the numerical uniaxial and biaxial curves in Figures 2 and 3. It can be noted from Figure 4 that the maximum tensile damage is about 0.88 which corresponds to a strain of 0.6×10^{-3}, whereas it shows a maximum compressive damage of 0.62 at a strain of 5×10^{-3}. As expected the material under compressive loading damages less and sustains more load than under tensile loading. Moreover, the same figure shows a maximum biaxial tensile damage of 0.65 at 0.7×10^{-3}, and a maximum compression damage of 0.75 at a strain of 7×10^{-3}. This indicates that in biaxial compression the material sustains more strains and as a result of that, higher values of damage occur than in the corresponding biaxial tension.

It is noteworthy to compare the damage evolution in both uniaxial and biaxial tensile/compressive loadings as shown in Figure 4. It can be seen that the largest evolution of damage occurs during uniaxial tension. Moreover, generally one can conclude that damage evolution during uniaxial tensile loading is higher than biaxial or multiaxial tensile loading. This can be attributed to geometrical constraints set by the evolution of cracks in different directions during biaxial or multiaxial loadings such that crack propagation can be suppressed by other propagating cracks.

Interaction between cracks may cause the material to harden such that a stronger response is obtained. However, an interesting behavior can also be noticed such that the previous conclusion cannot be inferred from the evolution of damage during uniaxial and biaxial compression. One can notice from Figure 4 that the amount of cracks generated during biaxial compression is higher than during uniaxial compression. This can be attributed to the amount of generated dilation and shear cracks (crushing) being larger during biaxial compression.

Three-point Bending Notched Beam

The problem described here illustrates the use of the proposed model for the analysis of a notched concrete beam under symmetric three-point loading. This problem is chosen because it has been studied extensively both experimentally and analytically. The predominant behavior is Mode I cracking, so this example provides a good verification of this aspect of the constitutive models. The sensitivity of the numerical results to the finite element discretization is investigated here.

The geometrical data of the notched beam are shown in Figure 5(a). The thickness of the beam is 102 mm. Because of symmetry, only one half of the beam is modeled by two meshes: Figure 5(b) shows the coarse mesh of 280 elements, and Figure 5(c) shows the a very fine mesh of 14,956 elements. The beam is modeled using four-noded plane stress (CPS4R) elements with reduced integration. The beam is loaded by prescribing a vertical displacement at the center of the beam until it reaches a value of 0.5 mm.

Since only damage in tension is activated in this example, only the material parameters defining the loading function in tension are of interest. Material parameters used in this example are: $\bar{E} = 21.7\,\text{GPa}$, $\nu = 0.2$, $f_0^+ = 2.4\,\text{MPa}$, $\alpha^{\text{p}} = 0.2$, $\alpha = 0.12$, $h = 3\,\text{GPa}$, $B^+ = 0.1$, and $\ell^+ = 20\,\text{mm}$. The material length scale ℓ^+ is determined by obtaining the closest agreement with the experimental data in Figure 6.

In Figure 6, the load versus load-point deflection curves from the simulation using the two meshes are compared with the experimental result of Malvar and Warren (1988). It can be noticed that no spurious mesh dependence is visible. Excellent agreement between predictions of the two meshes is observed through all loading stages: elastic, hardening, and softening. The numerical results also agree very well with the experimental result, which demonstrates the soundness of the present algorithm. The evolution of the damage zone, simulating the formation of a macrocrack leading to failure, is shown in Figure 7 for the fine mesh. In the first stage of the fracture process, damage is initiated at the left corner of the notch. The damage induced crack propagation path tends to curve away from the

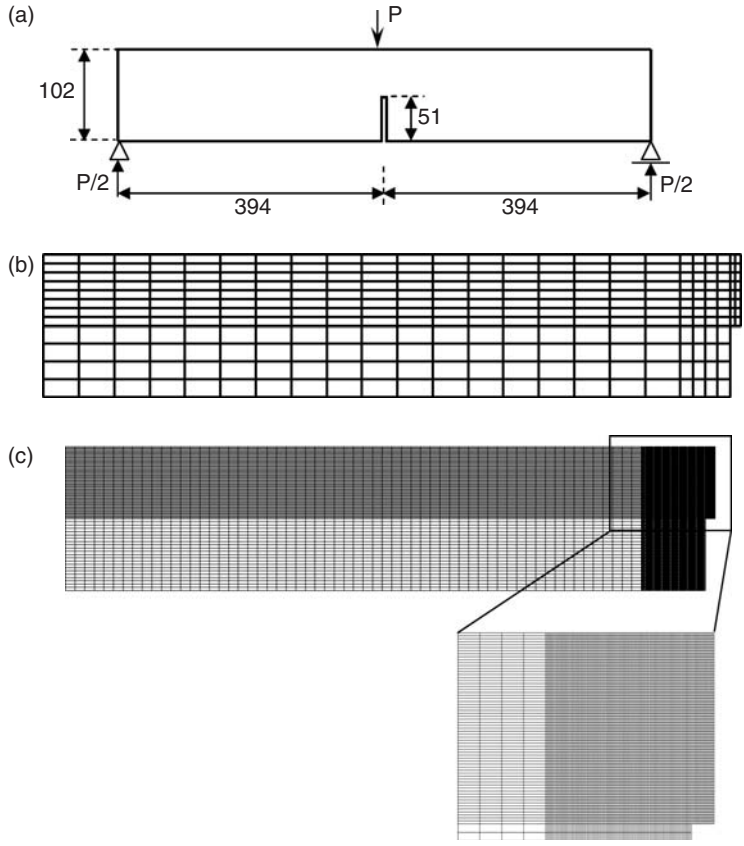

Figure 5. *Geometry and finite element meshes of the three-point bending notched beam: (a) geometry in mm, (b) coarse mesh, (c) fine mesh.*

original notch tip. This behavior agrees with the experimental observations. Moreover, the curved damage zone obtained indicates that the nonlocal-enhanced model is also insensitive to the orientation of the finite element mesh. This is an important aspect as mesh size objectivity, since the tendency of classical models to follow the mesh orientation may result in incorrect or even nonphysical crack patterns.

It is noteworthy that since the fracture mechanism in this problem is essentially Mode I and the friction or aggregate interlock does not play an important role, the introduction of damage-induced anisotropy does not seem to provide substantial advantages. Therefore, an isotropic damage model is sufficiently accurate.

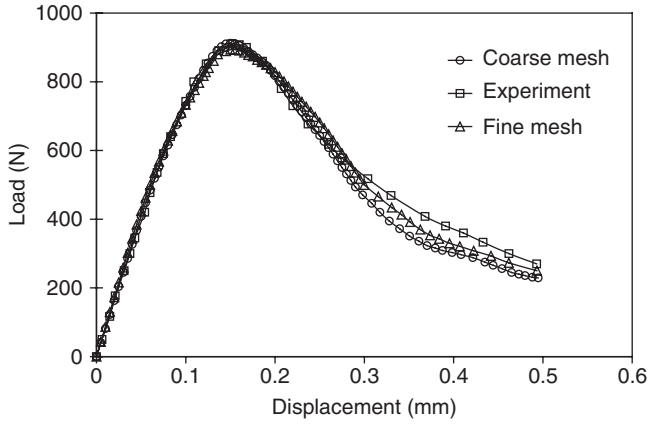

Figure 6. *Comparison of the load vs displacement for mesh refinement of the three-point bending notched beam. Experimental data by Malvar and Warren (1988).*

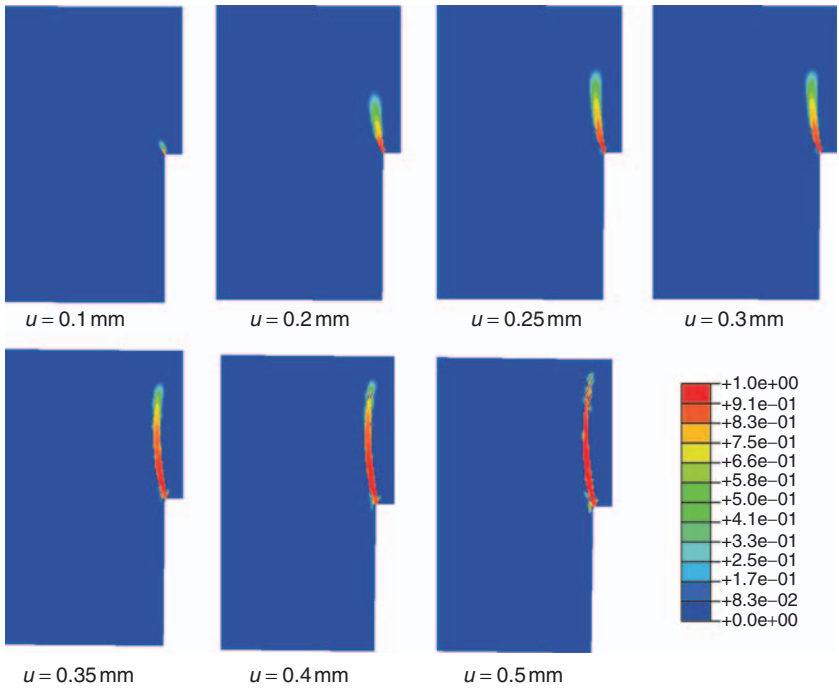

Figure 7. *Detail of the damage pattern evolution in the fine mesh around the notch as a function of the applied displacement u. Contours of the nonlocal equivalent tensile damage* $\widehat{\omega}^{+}$.

Four-point Bending Notched Beam

The second problem described here illustrates the use of the proposed model for the analysis of a four-point bending notched concrete beam subjected to loading that causes mixed-mode cracking. This problem has been chosen because it has been studied extensively both experimentally by Arrea and Ingraffea (1982) and repeated by many others, and analytically studied by many authors. The behavior in this problem is a combination of Mode I and Mode II cracking. It, therefore, provides verification of the proposed damage anisotropy for general mixed-mode loading. The sensitivity of the numerical results to the finite element discretization is also investigated here.

Since only damage in tension is activated in this example, only the material parameters defining the loading function in tension are of interest. Material parameters used in this example are: $\bar{E} = 23\,\text{GPa}$, $\nu = 0.18$, $f_0^+ = 2.6\,\text{MPa}$, $\alpha^p = 0.2$, $\alpha = 0.12$, $h = 8.5\,\text{GPa}$, $G_f^+ = 55\,\text{N/m}$, and $\ell^+ = 20\,\text{mm}$. The material length scale ℓ^+ is determined by obtaining the closest agreement with the experimental data of Arrea and Ingraffea (1982).

The geometry of the four-point notched beam is shown in Figure 8(a) with beam thickness of 156 mm. Figures 8(b) and (c) show the two meshes used for this problem: a coarse mesh of 210 elements, and a fine mesh of 840 elements. The beam is assumed to be in a state of plane stress, so four-noded (CPS4R) elements with reduced integration are used. The beam is loaded by applying a displacement u that increases linearly from zero to 0.12 mm. The displacement is applied at point C and transmitted to the notched beam through the rigid steel beam to points A and B. The load transmitted at points A and B is distributed over a 30 mm length to avoid hourglassing of the elements in the vicinity of these points where the highest loads are transmitted. The finite element modeling of this example has been fully described in ABAQUS (2003); therefore, the reader is referred to the manuals of ABAQUS for more details.

The response of the load transmitted at point A versus the crack mouth sliding displacement (CMSD) of the notched beam obtained with the two meshes is shown in Figure 9 together with the experimental data taken from Arrea and Ingraffea (1981). The CMSD is defined as the relative vertical displacement of the notch faces at the bottom of the beam. Figure 9 shows that the coarse and fine meshes give similar results which are in quite good agreement with the experimental results. The deformation pattern obtained at the end of the analysis is shown for the two meshes in Figure 10. It can be seen that the size of the damaged zone is

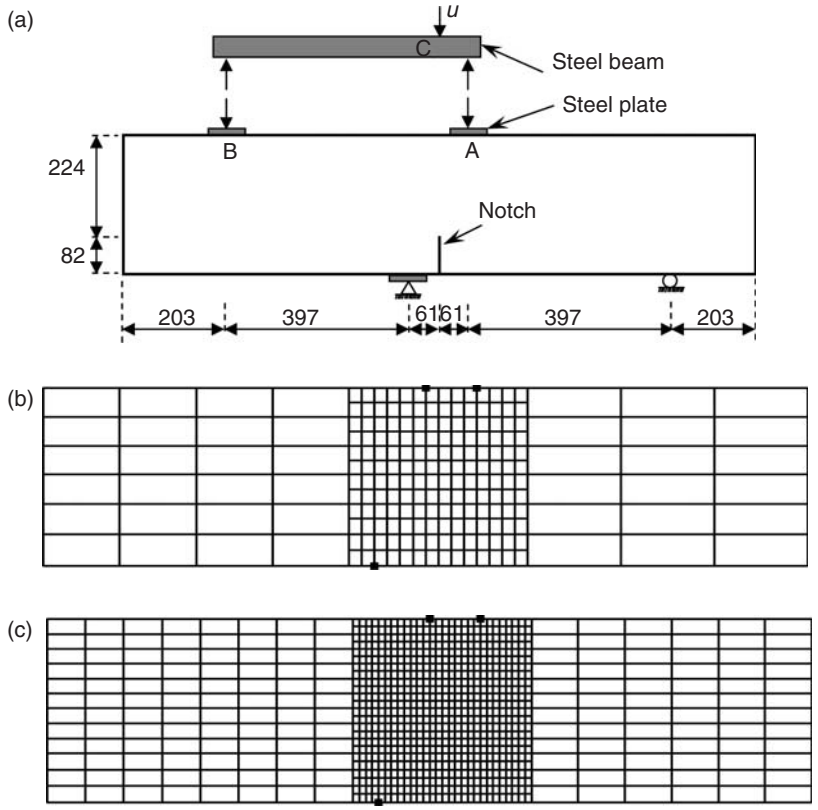

Figure 8. *Geometry and finite element meshes of the four-point bending notched beam: (a) geometry in mm, (b) coarse mesh, (c) fine mesh.*

almost mesh independent such that the nonlocal model allows for a spread of the damage over all the finite elements belonging to a zone whose dimensions are fixed by the material length scale and not by the element size. The evolution of the damage zone, simulating the formation of a macrocrack leading to failure, is shown in Figure 11 for the fine mesh. The damage induced crack propagation path tends to curve away from the original notch tip and move toward point A. This behavior is typical for a crack subjected to mixed-mode loading. Furthermore, the curved crack shape shows that the direction of damage growth and thus the final damage distribution are not affected by the orientation of the finite element mesh.

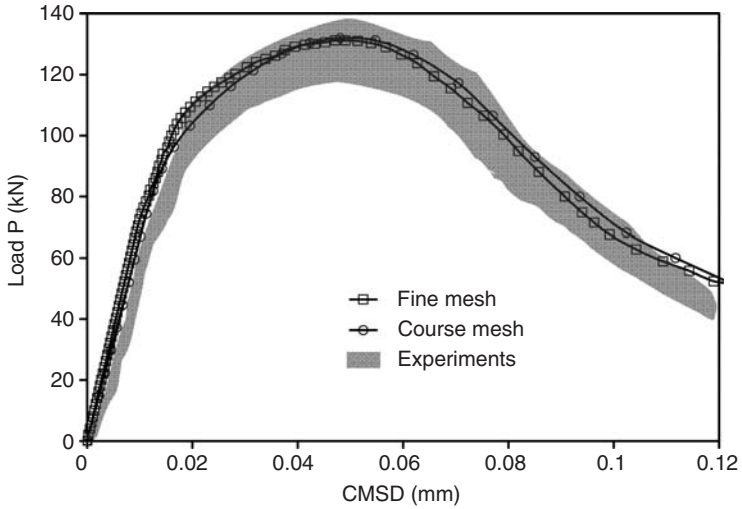

Figure 9. *Comparison of the load vs CMSD for mesh refinement of the four-point bending notched beam. Experimental data by Arrea and Ingraffea (1981).*

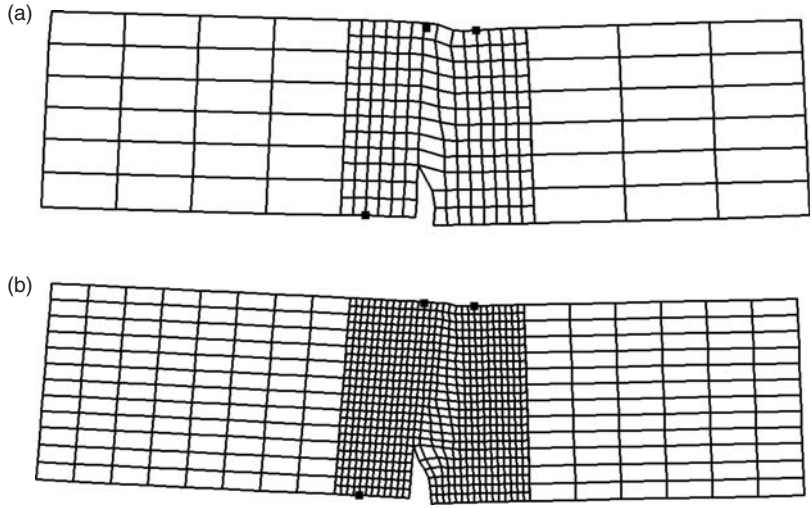

Figure 10. *Deformation patterns at failure obtained in mesh refinement: (a) coarse mesh, (b) fine mesh. Displacements have been scaled by a factor of 100.*

CONCLUSIONS

A nonlocal coupled plasticity-damage model for plain concrete is presented in this work. Based on continuum damage mechanics, a nonlocal

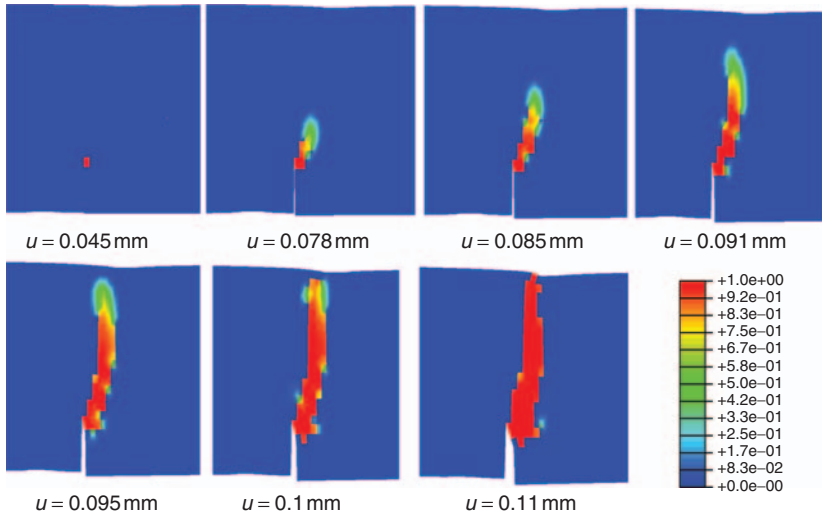

Figure 11. *Detail of the damage pattern evolution in the fine mesh around the notch as a function of the applied displacement u. Contours of the nonlocal equivalent tensile damage* $\bar{\omega}^{+}$.

gradient-enhanced anisotropic damage evolution is considered. The plasticity and damage loading surfaces account for both compressive and tensile loadings such that the tensile and compressive damages are characterized independently. The plasticity yield surface is expressed in the effective (undamaged) configuration, which leads to a decoupled algorithm for the effective stress computation and the nonlocal damage evolution. Two internal length scales have been introduced as localization limiters of damage in tension and compression. Numerical algorithm is presented for the implementation of the proposed model in the well-known finite element code ABAQUS via the material user subroutine UMAT.

The effectiveness of the proposed local model is demonstrated in both uniaxial and biaxial tension and compression problems and compared with experimental data (Cicekli et al., 2007).

The mesh objectivity of the gradient-enhanced damage approach is demonstrated by the application to two concrete fracture experiments: a three-point loading notched beam under Mode I fracture, and an anti-symmetric four-point loading notched beam under mixed mode (Modes I and II) fracture. Both the initiation and the propagation of damage can be simulated with greatly reduced mesh dependence of numerical results. Instead of localization in the smallest possible zone, as observed in classical continua, a damage band emerges which is several elements wide if the discretization is sufficiently fine. As a result, the global response is

insensitive to the mesh refinement such that a finite, nonzero fracture energy is obtained.

For the problems discussed in this work, the introduction of unilateral effect does not seem to provide substantial advantages, not even in the anti-symmetric four-point loading notched beam, since failure is dominated by tensile stresses. Hence, application of the proposed model to problems where unilateral effect is important will be presented in a future work.

The simplicity of the numerical implementation of the proposed model, in particular the calculation of the higher order gradients, and the simplicity of updating the effective stress, for which the classical return mapping algorithm is used, make the proposed model easy to be adapted for structural problems involving large computations as compared to the existing nonlocal damage models in the literature. However, the correct identification of the intrinsic material length scales from experimental tests still remains an open question and further work is needed in this direction.

REFERENCES

ABAQUS (2003). *Version 6.3, Habbitt*, Karlsson Fand Sorensen, Inc, Providence, RI.

Abu Al-Rub, R.K. (2004). Material Length Scales in Gradient-Dependent Plasticity/Damage and Size Effects: Theory and Computation, Ph.D. Dissertation, Louisiana State University, Louisiana, USA.

Abu Al-Rub, R.K. and Voyiadjis, G.Z. (2003). On the Coupling of Anisotropic Damage and Plasticity Models for Ductile Materials, *Int. J. Solids Struct.*, **40**: 2611–2643.

Abu Al-Rub, R.K. and Voyiadjis, G.Z. (2005). A Direct Finite Element Implementation of the Gradient Plasticity Theory, *Int. J. Numer. Meth. Engng*, **63**: 603–629.

Abu Al-Rub, R.K. and Voyiadjis, G.Z. (2006). A Finite Strain Plastic-Damage Model for High Velocity Impacts Using Combined Viscosity and Gradient Localization Limiters, Part I: Theoretical Formulation, *Int. J. Damage Mech.*, **15**(4): 293–334.

Aifantis, E.C. (1984). On the Microstructural Origin of Certain Inelastic Models, *J. Eng. Mater. Tech.*, **106**: 326–330.

Ananiev, S. and Ozbolt, J. (2004). Plastic-damage Model for Concrete in Principal Directions, In: Li, V., Leung, C.K.Y., William, K.J. and Billington, S.L. (eds), *Fracture Mechanics of Concrete Structures*, pp. 271–278, Colorado, USA.

Arrea, M. and Ingraffea, A.R. (1982). Mixed-mode Crack Propagation in Mortar and Concrete, Report No. 81–13, Department of Structural Engineering, Cornell University, Ithaca, NY.

Askes, H., Pamin, J. and de Borst, R. (2000). Dispersion Analysis and Element-Free Galerkin Solutions of Second- And Fourth-Order Gradient Enhanced Damage Models, *Int. J. Numer. Meth. Engng*, **49**: 811–832.

Bazant, Z.P. and Kim, S.-S. (1979). Plastic-fracturing Theory for Concrete, *ASCE J. Eng. Mech.*, **105**: 407–28.

Bazant, Z.P. and Pijaudier-Cobot, T.G.P. (1988). Nonlocal Continuum Damage, Localization Instability and Convergence, *J. Appl. Mech.*, **55**: 287–293.

Bazant, Z.P. and Pijaudier-Cabot, T.G.P. (1989). Measurement of Characteristic Length of Non-Local Continuum, *ASCE J. Eng. Mech.*, **115**: 755–767.

Carol, I., Rizzi, E. and William, K.J. (2001). On the Formulation of Anisotropic Elastic Degradation. Ii. Generalized Pseudo-rankine Model for Tensile Damage, *Int. J. Solids Struct.*, **38**: 519–546.

Chen, J. and Yuan, H. (2002). A Micro-Mechanical Damage Model Based on Gradient Plasticity: Algorithms and Applications, *Int. J. Numer. Meth. Engng*, **54**: 399–420.

Chow, C.L. and Wang, J. (1987). An Anisotropic Theory of Elasticity for Continuum Damage Mechanics, *International Journal of Fracture*, **33**: 2–16.

Cicekli, U., Voyiadjis, G.Z. and Abu Al-Rub, R.K. (2007). A Plasticity and Anisotropic Damage Model for Plain Concrete, *Int. J. Plasticity*, **23**: 1874–1900.

Comi, C. and Perego, U. (1996). A Generalized Variable Formulation for Gradient Dependent Softening Plasticity, *Int. J. Numer. Meth. Engng*, **39**: 3731–3755.

Comi, C. (2001). A Non-Local Model with Tension and Compression Damage Mechanisms, *Eur. J. Mech. A/Solids*, **20**: 1–22.

Cordebois, J.P. and Sidoroff, F. (1979). Anisotropic Damage in Elasticity and Plasticity, *Journal de Mecanique Theorique et Applilquee*, Numero Special, 45–40.

de Borst, R. and Mühlhaus, H.-B. (1992) Gradient-dependent Plasticity Formulation and Algorithmic Aspects, *Int. J. Numer. Methods Engrg.*, **35**: 521–539.

de Borst, R., Sluys, L.J., Mühlhaus, H.-B. and Pamin, J. (1993). Fundamental Issues in Finite Element Analysis of Localization Of Deformation, *Engineering Computations*, **10**: 99–121.

de Borst, R. and Pamin, J. (1996). Some Novel Developments in Finite Element Procedures for Gradient Dependent Plasticity, *Int. J. Numer. Methods Engrg.*, **39**: 2477–2505.

de Borst, R., Pamin, J. and Geers, M. (1999). On Coupled Gradient-Dependent Plastcity and Damage Theories with A View to Localization, *Eur. J. Mech. A/Solids*, **18**: 939–962.

Dragon, A. and Mroz, Z. (1979). A Continuum Model for Plastic-Brittle Behavior of Rock and Concrete, *International Journal of Engineering Science*, **17**: 121–137.

Faria, A., Oliver, J. and Cervera, M. (1998). A Strain-based Plastic Viscous-damage Model for Massive Concrete Structures, *Int. J. Solids Struct.*, **35**: 1533–1558.

Ferrara, L. and di Prisco, M. (2001). Mode I Fracture Behavior in Concrete: Nonlocal Damage Modeling, *ASCE J. Eng. Mech.*, **127**: 678–692.

Fichant, S., Borderie, C.L. and Pijaudier-Cabot, G. (1999). Isotropic and Anisotropic Descriptions of Damage in Concrete Structures, *Mech. Cohes.-Frict. Mater.*, **4**: 339–359.

Gatuingt, F. and Pijaudier-Cabot, G. (2002). Coupled Damage and Plasticity Modeling in Transient Dynamic Analysis of Concrete, *Int. J. Numer. Anal. Meth. Geomech.*, **26**: 1–24.

Geers, M.G.D., Peerlings, R.H.J., Brekelmans, W.A.M. and de Borst, R. (2000). Phenomenological Nonlocal Approaches Based on Implicit Gradient-enhanced Damage, *Acta Mechanica*, **144**: 1–15.

Gudmundson, P. (2004). A Unified Treatment of Strain Gradient Plasticity, *J. Mech. Phys. Solids*, **52**: 1379–1406.

Govindjee, S., Kay, G.J. and Simo, J.C. (1995). Anisotropic Modelling and Numerical Simulation of Brittle Damage In Concrete, *Int. J. Numer. Meth. Engng*, **38**: 3611–3633.

Halm, D. and Dragon, A. (1996). A Model of Anisotropic Damage by Mesocrack Growth; Unilateral Effect, *Int. J. Damage Mech.*, **5**: 384–402.

Hansen, E., William, K. and Carol, I. (2001). A Two-surface Anisotropic Damage/Plasticity Model for Plain Concrete, In: de Borst, R., Mazars, J., Pijaudier-Cabot, G. and van Mier, J.G.M. (eds), *Fracture Mechanics of Concrete Structures*, pp. 549–556, Balkema, Lisse.

Imran, I. and Pantazopoulu, S.J. (2001). Plasticity Model For Concrete Under Triaxial Compression, *ASCE J. Eng. Mech.*, **127**: 281–290.

Jansen, D.C. and Shah, S.P. (1997). Effect of Length on Compressive Strain Softening of Concrete, *ASCE J. Eng. Mech.*, **123**: 25–35.

Jason, L., Pijaudier-Cabot, G., Huerta, A., Crouch, R. and Ghavamian, S. (2004). An Elastic Plastic Damage Formulation for the Behavior of Concrete, In: Li, V., Leung, C.K.Y., William, K.J. and Billington, S.L. (eds), *Fracture Mechanics of Concrete Structures*, pp. 549–556, Colorado, USA.

Jason, L., Huerta, A., Pijaudier-Cabot, G. and Ghavamian, S. (2006). An Elastic Plastic Damage Formulation for Concrete: Application to Elementary Tests and Comparison with an Isotropic Damage Model, *Comput. Methods Appl. Mech. Engrg.*, **195**: 7077–7092.

Ju, J.W. (1989). On Energy-based Coupled Elasto-plastic Damage Theories: Constitutive Modeling and Computational Aspects, *Int. J. Solids Struct.*, **25**: 803–833.

Ju, J.W. (1990). Isotropic and Anisotropic Damage Variables in Continuum Damage Mechanics, *ASCE J. Eng. Mech.*, **116**: 2764–2770.

Kachonov, L.M. (1958). On the Creep Fracture Time, *Izv. Akad. Nauk USSR Otd. Tech.*, **8**: 26–31 (in Russian).

Karsan, I.D. and Jirsa, J.O. (1969). Behavior of Concrete under Compressive Loadings, *J. Struct. Div., ASCE*, **95**: 2535–2563.

Krajcinovic, D. and Fonseka, G.U. (1981). The Continuous Damage Theory of Brittle Materials. Part I: General Theory, *J. Appl. Mech.*, **48**: 809–815.

Krajcinovic, D. (1983). Continuum Damage Mechanics, *Applied Mechanics Reviews*, **37**: 1–6.

Krajcinovic, D. (1985). Continuous Damage Mechanics Revisited: Basic Concepts and Definitions, *J. Appl. Mech.*, **52**: 829–834.

Krajcinovic, D. (1996). *Damage Mechanics*, North-Holland, Amsterdam.

Kratzig, W. and Polling, R. (2004). An Elasto-plastic Damage Model for Reinforced Concrete With Minimum Number of Material Parameters, *Computers and Structures*, **82**: 1201–1215.

Kuhl, E., Ramm, E. and de Borst, R. (2000). An Anisotropic Gradient Damage Model for Quasi-brittle Materials, *Comput. Methods Appl. Mech. Engrg.*, **183**: 87–103.

Lemaitre, J. (1992). *A Course on Damage Mechanics*, Springer, Berlin.

Lasry, D. and Belytschko, T. (1988). Localization Limiters in Transient Problems, *Int. J. Solids Struct.*, **24**: 581–597.

Lee, J. and Fenves, G.L. (1998). A Plastic-damage Model for Cyclic Loading of Concrete Structures, *ASCE J. Eng. Mech.*, **124**: 892–900.

Liebe, T., Menzel, A. and Steinmann, P. (2003). Theory and Numerics of Geometrically Non-linear Gradient Plasticity, *Int. J. Eng. Sci.*, **41**: 1603–1629.

Lubarda, V.A. and Krajcinovic, D. (1993). Damage Tensors and the Crack Density Distribution, *Int. J. Solids Struct.*, **30**: 2859–2877.

Lubarda, V.A., Kracjinvovic, D. and Mastilovic, S. (1994). Damage Model for Brittle Elastic Solids with Unequal Tensile and Compressive Strength, *Engineering Fracture Mechanics*, **49**: 681–697.

Lubliner, J., Oliver, J., Oller, S. and Onate, E. (1989). A Plastic-damage Model for Concrete, *Int. J. Solids Struct.*, **25**: 299–326.

Malvar, L.J. and Warren, G.E. (1988). Fracture Energy for Three-point Bend Tests on Single-edge Notched Beams, *Experimental Mechanics*, **45**: 266–272.

Matsushima, T., Chambon, R. and Caillerie, D. (2002). Large Strain Finite Element Analysis of a Local Second Gradient Model: Application To Localization, *Int. J. Numer. Meth. Engng*, **54**: 499–521.

Mazars, J. and Pijaudier-Cabot, G. (1989). Continuum Damage Theory: Application to Concrete, *ASCE J. Eng. Mech.*, **115**: 345–365.

Meschke, G., Lackner, R. and Mang, H. (1998). An Anisotropic Elastoplastic-damage Model for Plain Concrete, *Int. J. Numer. Meth. Engng*, **42**: 703–727.

Mikkelsen, L.P. (1997). Post-necking Behavior Modeling by a Gradient Dependent Plasticity Theory, *Int. J. Solids Struct.*, **34**: 4531–4546.

Mühlhaus, H.B. and Aifantis, E.C. (1991). A Variational Principle for Gradient Principle, *Int. J. Solids Struct.*, **28**: 845–857.

Murakami, S. and Ohno, N. (1981). A Continuum Theory of Creep And Creep Damage, In: *Proceedings of the Third IUTAM Symposium on Creep in Structures*, pp. 422–444, Springer, Berlin.

Nedjar, B. (2001). Elastoplastic-Damage Modeling Including the Gradient of Damage: Formulation and Computational Aspects, *Int. J. Solids Struct.*, **38**: 5421–5451.

Onate, E., Oller, Oliver, S. and Lubliner, J. (1988). A Constitutive Model of Concrete Based on the Incremental Theory of Plasticity, *Engineering Computations*, **5**: 309–319.

Ortiz, M. (1985). A Constitutive Theory for the Inelastic Behavior of Concrete, *Mech. Mat.*, **4**: 67–93.

Pamin, J. (1994). Gradient-Dependent Plasticity in Numerical Simulation of Localization Phenomena, Dissertation, Delft University of Technology.

Pamin, J., Askes, H. and de Borst, R. (2003). Two Gradient Plasticity Theories Discretized with the Element-free Galerkin Method, *Comput. Methods Appl. Mech. Engrg.*, **192**: 2377–2403.

Peerlings, R.H.J., de Borst, R., Brekelmans, W.A.M. and de Vree, J.H.P. (1996). Gradient Enhanced Damage for Quasi-brittle Materials, *Int. J. Numer. Methods in Engrg.*, **39**: 3391–3403.

Peerlings, R.H.J., de Borst, R., Brekelmans, W.A.M. and Geers, M.G.D. (1998). Gradient-enhanced Damage Modelling of Concrete Fracture, *Mech. Cohes.-Frict. Mater.*, **3**: 323–342.

Pijaudier-Cabot, G. and Bazant, Z.P. (1987). Nonlocal Damage Theory, *ASCE J. Eng. Mech.*, **113**: 1512–1533.

Ramaswamy, S. and Aravas, N. (1998a). Finite Element Implementation of Gradient Plasticity Models. Part I: Gradient-dependent Yield Functions, *Comput. Methods Appl. Mech. Engrg.*, **163**: 11–32.

Ramaswamy, S. and Aravas, N. (1998b). Finite Element Implementation of Gradient Plasticity Models. Part II: Gradient-dependent Evolution Equations, *Comput. Methods Appl. Mech. Engrg.*, **163**: 33–53.

Ramtani, S., Berthaud, Y. and Mazars, J. (1992). Orthotropic Behavior of Concrete with Directional Aspects: Modelling and Experiments, *Nuclear Eng. Design*, **133**: 97–111.

Sidoroff, F. (1981). Description of Anisotiopic Damage Application to Elasticity, In: *IUTAM Colloqium on Physical Nonlinearities in Structural Analysis*, pp. 237–244, Springer-Verlag, Berline.

Simo, J.C. and Ju, J.W. (1987a). Strain and stress-based continuum damage. Model. Part I: Formulation, *Int. J. Solids Struct.*, **23**: 821–840.

Simo, J.C. and Ju, J.W. (1987b). Strain- and Stress-based Continuum Damage Models. Part II: Computational Aspects, *Int. J. Solids Struct.*, **23**: 841–869.

Simo, J.C. and Hughes, T.J.R. (1998). Computational Inelasticity, In: *Interdisciplanary Applied Mathematics*, Springer, New York.

Svedberg, T. and Runesson, K. (2000). An Adaptive Finite Element Algorithm for Gradient Theory of Plasticity with Coupling to Damage, *Int. J. Solids Struct.*, **37**: 7481–7499.

Valanis, K.C. (1991). A Global Damage Theory and the Hyperbolicity of the Wave Problem, *J. Appl. Mech.*, **58**: 311–316.

Voyiadjis, G.Z. and Abu-Lebdeh, T.M. (1994). Plasticity Model for Concrete Using the Bounding Surface Concept, *Int. J. Plasticity*, **10**: 1–21.

Voyiadjis, G.Z. and Kattan, P.I. (1999). *Advances in Damage Mechanics: Metals and Metals Matrix Composites*, Elsevier, Oxford.

Voyiadjis, G.Z., Deliktas, B. and Aifantis, E.C. (2001). Multiscale Analysis of Multiple Damage Mechanics Coupled With Inelastic Behavior of Composite Materials, *ASCE J. Eng. Mech.*, **127**: 636–645.

Voyiadjis, G.Z., Abu Al-Rub, R.K. and Palazotto, A.N. (2003). Non-local Coupling of Viscoplasticity and Anisotropic Viscodamage for Impact Problems Using the Gradient Theory, *Archives of Mechanics*, **55**: 39–89.

Voyiadjis, Z.V., Abu Al-Rub, K.R. and Palazotto, A.N. (2004). Thermodynamic Framework for Coupling of Non-local Viscoplasticity and Non-local Anisotropic Viscodamage for Dynamic Localization Problems Using Gradient Theory, *Int. J. Plasticity*, **20**: 981–1038.

Voyiadjis, G.Z. and Abu Al-Rub, R.K. (2006). A Finite Strain Plastic-damage Model for High Velocity Impacts Using Combined Viscosity and Gradient Localization Limiters, Part II: Numerical Aspects and Simulations, *Int. J. Damage Mech.*, **15**: 335–373.

Wu, J.U., Li, J. and Faria, R. (2006). An Energy Release Rate-based Plastic-damage Model for Concrete, *Int. J. Solids Struct.*, **43**: 583–612.

Yazdani, S. and Schreyer, H.L. (1990). Combined Plasticity and Damage Mechanics Model for Plain Concrete, *ASCE J. Eng. Mech.*, **116**: 1435–1450.

Zbib, H.M. and Aifantis, E.C. (1992). On the Gradient-dependent Theory of Plasticity and Shear Banding, *Acta Mechanica*, **92**: 209–225.

Zervos, A., Papanastasious, P. and Vardoulakis, I. (2001). A Finite Element Displacement Formulation for Gradient Elastoplasticity, *Int. J. Numer. Meth. Engng*, **50**: 1369–1388.